Universidade de Aveiro Departamento de Engenharia Mecânica
2013

Daniel Rodrigues Jesus Fernandes

Estudo comparativo de geradores eletromagnéticos para prótese de anca

Universidade de Aveiro Departamento de Engenharia Mecânica
2013

Daniel Rodrigues Jesus Fernandes

Estudo comparativo de geradores eletromagnéticos para prótese de anca

Dissertação apresentada à Universidade de Aveiro para cumprimento dos requisitos necessários à obtenção do grau de Mestre em Engenharia Mecânica, realizada sob a orientação científica de Jorge Augusto Fernandes Ferreira, Professor Auxiliar do Departamento de Engenharia Mecânica da Universidade de Aveiro e de António Manuel de Amaral Monteiro Ramos, Professor Auxiliar do Departamento de Engenharia Mecânica da Universidade de Aveiro.

O júri

Presidente	Prof. Doutor António Manuel Godinho Completo Professor Auxiliar do Departamento de Engenharia Mecânica da Universidade de Aveiro
Arguente	Prof. Doutor Carlos Alberto da Costa Bastos Professor Auxiliar do Departamento de Eletrónica, Telecomunicações e Informática da Universidade de Aveiro
Orientador	Prof. Doutor Jorge Augusto Fernandes Ferreira Professor Auxiliar do Departamento de Engenharia Mecânica da Universidade de Aveiro

Agradecimentos / Acknowledgements

Deixo a sincera gratidão ao Prof. Jorge Ferreira pela sua paciência, acompanhamento e disponibilidade para me guiar durante este projeto.

Ao Prof. António Ramos pelos conhecimentos na área de dispositivos biomecânicos que me transmitiu.

Ao Mestre Marco Santos pelo seu apoio permanente em todos os aspetos do trabalho.

Ao Prof. Pascoal pela constante crítica construtiva e boa disposição.

Ao Sr. Rafeiro pela sua transmissão de conhecimento na área de construção mecânica, e aos meus colegas Telmo Rafeiro, João Torrão, Diogo Grilo e João Moura pela assistência em algumas dificuldades.

Aos meus colegas, amigos de óleo, que reciprocamente me apoiaram na formação académica.

Ao Nuno, ao Francisco, à Bárbara, ao Luís, à Sara, ao João e à Joana a quem tenho o prazer de chamar amigos.

Aos meus pais e às minhas pequenas que apesar de tudo estão sempre aqui.

Palavras-chave Geração de energia, prótese de anca, geradores eletromagnéticos.

Resumo

A necessidade de substituir os tradicionais métodos de alimentação de dispositivos médicos instrumentados implantáveis, baseados em baterias, por sistemas alternativos de durabilidade superior conduziu à crescente investigação nesta área.

Após a verificação precedente desta dissertação do melhor desempenho da indução eletromagnética relativamente a outros sistemas de geração de energia, partindo do movimento humano, este trabalho descreve a conceção e avaliação comparativa de geradores eletromagnéticos, focado na implementação destes em próteses de anca em pacientes.

Estes foram criados com o objetivo de operar sob movimento análogo ao da anca humana, tanto em regime de repetibilidade, recorrendo a um manipulador robótico, como em regime empírico, acoplando-o à zona da anca de um indivíduo.

Uma análise comparativa foi efetuada entre diversas configurações de geradores com o intuito de, no futuro, uma otimização recorrente a modelos matemáticos não lineares seja validada e aplicada.

Os resultados revelaram que a extrapolação dos dados obtidos pelos ensaios realizados no manipulador para o ciclo de marcha humano contínuo apresentou um grau considerável de discrepância para com o teste empírico. O melhor ensaio do manipulador, obtido ao longo de um período de marcha, quando multiplicado por $2{,}5$ ciclos perfaz um total de $1{,}48\mu J$, enquanto o ensaio empírico gerou $67{,}3\mu J$ durante os mesmos $2{,}5$ ciclos de marcha.

Considerando que o ensaio de marcha executado empiricamente apresenta movimento aproximadamente equivalente ao do interior de uma prótese de anca, verificou-se a geração de energia considerável para alimentar um implante inteligente, ainda que as dimensões do gerador testado sejam ainda relativamente elevadas.

Keywords Energy harvesting, hip prosthesis, electromagnetic generators.

Abstract

The need of replacing traditional methods of feeding implantable instrumented medical devices, based on batteries, by alternative systems of superior lifetime led to an increasing investigation in this area.

After the verification, preceding this dissertation, of the electromagnetic induction better performance relatively to other energy harvesting systems using human motion, this work describes the conception and comparative evaluation of electromagnetic generators, focused on their implementation in hip prostheses on patients.

A comparative analysis was performed between different generator configurations, with the goal of, in the future, validating and applying an optimization resorting to non linear mathematical models.

These were created with the goal of operating under motion analogous to the human hip, in either a state of repeatability, resorting to a robotic manipulator, as in empiric state, attaching it to one's hip.

The results revealed that the extrapolation of the obtained data from the trials obtained from the manipulator into a continuous human gait cycle presented a considerable degree of discrepancy with the empiric test. The best manipulator trial, obtained from one gait cycle period, when multiplied by $2{,}5$ cycles totals a harvested energy of $1{,}48\mu J$, whilst the empiric rehearsal generated $67{,}3\mu J$ over the same $2{,}5$ gait cycle periods.

Considering that the walking rehearse tested empirically presents motion approximately equivalent to the interior of a hip prosthesis, considerable energy harvesting to feed an intelligent implant was verified, although the tested generator's dimensions are still relatively large.

Index

Index of Figures

Index of Tables

Symbology / Acronyms

$\boldsymbol{IMDs}$	Implantable Medical Devices
$\boldsymbol{AIMDs}$	Active Implantable Medical Devices
$\boldsymbol{LiI_2}$	Lithium Iodine compound
$\boldsymbol{O_2}$	Oxygen molecule
$\boldsymbol{pH}$	Power of Hydrogen
$\boldsymbol{TEG}$	Thermoelectric Generator
$\boldsymbol{PVDF}$	Polyvinylidene Fluoride
$\boldsymbol{PZT}$	Lead Zirconium Titanate
$\boldsymbol{emf}$	Electromotive Force

Chapter 1

Introduction

This chapter fits the dissertation context as well as the objectives pretended with its development.

1.1 Project Context

This work is conducted within the project PTDC/EME-PME/105465/2008: Sistema de Alimentação Fisiológica para Avaliação In Vivo do Comportamento de Implantes Ósseos.

This dissertation is framed in a more embracing objective which is the one of conceiving a smart prosthesis capable of detecting problems occurred in its interface with the surrounding bone and, under external medical follow-in, capable of implementing prophylactic and/or corrective therapies.

The electric powering of Active Implantable Medical Devices (AIMDs) in the human body has critical issues that are not yet fully solved.

Many progresses have been proposed to develop energy harvesting systems in order to power electronic devices inside AIMDs.

Body-worn or implanted sensor systems are increasingly used in medical electronics and wearable computing.

In these applications, long lifetime and low maintenance power sources are usually required. Existing solutions such as primary or secondary batteries cannot satisfy these requirements [1].

A promising alternative to these finite lifetime power sources is the extraction and conversion of the energy from one's daily movements using body-implemented devices.

A previous dissertation in the scope of this project has proven the better performance of electromagnetic generators (specifically a mass-spring system) over piezoelectric components [2].

Being so, this work focuses on exploiting the electromagnetic principle to harvest energy inside implantable medical devices.

1.2 Main objectives

This work aims for the development and testing of electrical energy generators, for smart hip prosthesis application. The electromagnetic principle will be used for this purpose.

Several configurations shall be proposed and tested, and the comparative study of the several solutions using typical human motion simulation shall be taken into account.

For the developed prototypes, tests which characterize the generated electrical energy inside the hip prosthesis should be performed.

In order to accomplish the above described objectives, the following main tasks are proposed:

1. State of the art review regarding to the latest developments in electromagnetic generation obtained from mechanical energy;
2. Project and development of prototypes for electric energy generation. The development of two different generator types is proposed: the mass-spring generator and the magnetic levitation generator;
3. Conductance of trials for testing the devices above mentioned.

1.3 Document Outline

The dissertation is arranged in six chapters in order to provide a progressive comprehension of the problem's concepts. The content can be synthesised the following way:

- Chapter 1 - Introduction
  - This chapter fits the dissertation context as well as the objectives pretended with its development.
- Chapter 2 – Literature Review
  - A presentation of some energy harvesting systems is made, as well as a more intensive analysis of the different electromagnetic systems developed so far.
- Chapter 3 – Methodology for comparative analysis
  - This chapter describes the proposed electromagnetic generators, their mechanical construction and the whole structure's. The whole

experimental setup for the preparation of the trials is also explained, with the respective data adjusting considerations.

- Chapter 4 – Experimental trials
  - Taking into account the proposed generators, their diverse configurations are specified in this chapter.
- Chapter 5 – Results and comparative analysis
  - This chapter exhibits the experimental results and their analysis in the context of the project objectives previously defined.
- Chapter 6 – Conclusions and future work
  - The work is finalized in this chapter, with comments and conclusions about the obtained results, in order to contextualize suggestions for future work and developments.

This synthesis can be found at the start of each chapter, with the purpose of providing an initial framing of these during the reading.

Chapter 2

Literature Review

A presentation of some energy harvesting systems is made, as well as a more intensive analysis of the different electromagnetic systems developed so far.

Over the last decades there has been a big progress in low-power technologies, leading to the intensive development of devices, enabling them to be mass produced at low cost. Also, the consecutive development of wireless communications has contributed to the production of electronic devices in many human activities [3].

Knowing so, an important issue to take into account is the feeding of these devices. Despite all the efforts in the electronic apparatus industry, none of their functions will be possible if the devices don't have energy supply.

Therefore, the familiarization with the main energy providing methods and systems is presented in the following section, centred on powering portable devices.

2.1 Energy harvesting systems

For a brief presentation of some energy harvesting systems, it is considered the most relevant ones in what comes to feeding implantable medical devices (IMDs), such as lithium batteries, bio-fuel cells, nuclear cells, thermoelectric generators, piezoelectric systems and electromagnetic generators.

The crushing majority of portable electronic devices is fed by lithium batteries, either rechargeable (secondary batteries) or non-rechargeable (primary batteries) [4]. These have the massive advantage of providing a high voltage as well as having a high energetic density.

Batteries are mostly composed of LiI_2 when meant to power implantable devices. One of the reasons for the big adherence to this type of system is their discharging

process, because the voltage changes gradually accordingly to the battery's remaining charge instead of abruptly, allowing enough time for their replacement [2].

Another source of energy is the bio-fuel cells. These are cells based on a Glicose/O_2 enzymatic compound, actuating on a neutral pH, and were firstly proposed by Yahiro et al in 1964 [5]. These cells provide a low energy density, in terms of comparison with batteries, although they are an important subject to analyse, since they use organic components as fuel which could be, for instance, within the human body as a way to produce energy to power a micro system.

A voltage of $0{,}52V$ and an electric current of $8{,}3\mu A$ were proven obtainable from this method, in a physiologic solution of $0{,}0026\ mm^3$ at a temperature of $37°C$. With an output power of $4{,}3\mu W$, the capability of operating implanted sensors is predicted, as well as the information transmission to the outside [6].

Nuclear batteries are as well a way of obtaining electrical energy. These batteries use the energy contained in particles that are emitted by radioactive elements. Nuclear cells have the advantages of having a long lifetime even when compared to lithium cells, have an excellent energetic density, and can produce stable energy practically unaffected by external factors like temperature, pressure or magnetic fields. These are although difficult to produce and have very high cost associated to them [7].

Another important point of attention is the thermoelectric generator (TEG), based on the Seebek effect in which a temperature difference between two dissimilar electrical conductors or semiconductors produces a voltage difference between the two substances. Theoretically, the expression that describes the voltage, when thermocouples are used, is discriminated in Equation 1.

$$V_{out} = n\Delta T(\alpha_1 - \alpha_2) \qquad (1)$$

$V_{out} - \ Output\ voltage$
$n - Number\ of\ parallel\ thermocouples$
$\Delta T - Temperature\ gradient$
$\alpha_1 - \ Seebek\ coefficient\ for\ material\ 1$
$\alpha_2 - \ Seebek\ coefficient\ for\ material\ 2$

For a generator that operates with the temperature gradient between the human body and the exterior ambient, the ΔT component will not surpass 4℃. Also, for low-cost materials, the component $\alpha_1 - \alpha_2$ should not exceed $150\mu V/k$. Thus, it is clear that in order to obtain a reasonable voltage, an extremely high number of thermocouples should be implemented.

However, in order to compete with batteries, this kind of device needs to be restricted in size and price.

The use of piezoelectric materials for obtaining energy is as well more and more frequent. Among the frequently used, Polyvinylidene Fluoride (PVDF) and Lead Zirconium Titanate (PZT) are the most exploited [8].

The use of these components as a source of energy in medical applications was proposed only recently. The practical challenges inherent to these applications (commonly low frequency systems) are essentially their high voltage, low electric current and high impedance, as well as relatively low power output [9]. Other questions such as efficiency, energy conditioning and storage are not yet completely solved. In addition, reduced dimensions and sometimes irregular shapes are also required.

Last but not least, the electromagnetic principle has as well been explored in biomechanical applications. This electric generation principle based on the known Faraday's law of induction, which says that an electromotive force (emf) can be induced in a circuit by changing a magnetic field [10].

As previously explained, this dissertation relies on electromagnetic systems, so a more detailed analysis over this topic is presented in the following section.

2.2 Developed micro electromagnetic systems

The ideal mass-spring generator (Figure 1) was firstly proposed by [11], merely studying the theoretical linear model and analyzing the feasibility of generating practical amounts of energy from mechanical vibrations in small devices. The concept consists of a magnet corresponding to the mass, attached to a spring which is fixed to a housing with a winded coil. As the housing moves, a relative movement between it and the magnet occurs and energy is generated (Faraday's law of induction).

This type of energy generation system has been studied by many other investigators since then, for different applications, taking [12] as an example where the analysis of the feasibility of a generator with input vibration sources was taken into account.

The opposite motion was also tried, specifically an axially magnetized permanent magnet configuration with a single phase moving coil composed by three alternate windings in series (Figure 2) [13].

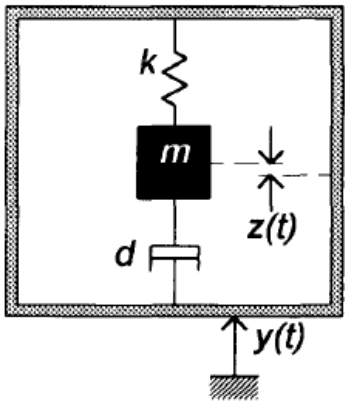

Figure 1 – Mass-spring system [11].

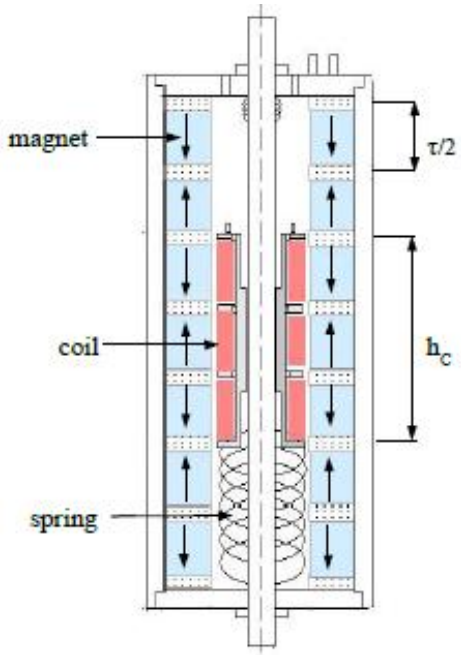

Figure 2 – Scheme of electromagnetic mechanically resonant generator [13].

As it is known, mechanical springs suffer from fatigue, regardless of their properties. Taken that into account, an alternative was proposed in [14], in which the functionality of the spring is replaced by a magnet. Three different configurations were tested (Figure 3) with axially magnetized permanent magnets placed vertically inside a Teflon tube so that facing surfaces have the same polarization. The moving magnet is repelled by the fixed weaker ones, that is, a levitation phenomena with a behaviour similar to a spring.

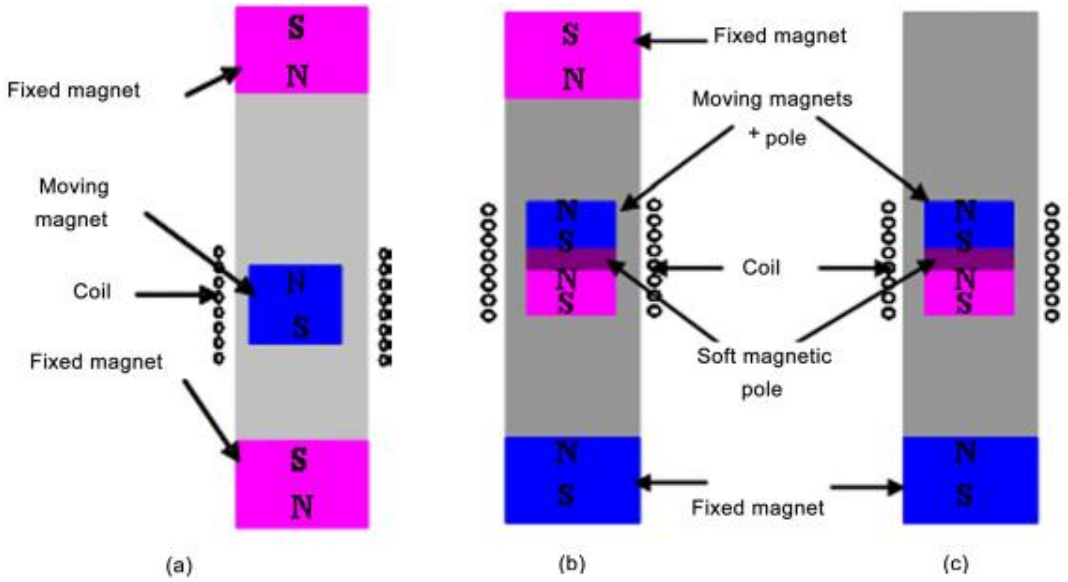

Figure 3 – Magnetic levitation generator structure (a) single moving magnet, (b) single moving magnet replaced two magnets + pole and (c) one fixed magnet [14].

Thereafter a new concept of micro-generator was described in [15], based on a planar pick-up coil and flexible polyimide membrane (Figure 4). The theoretical approach was still assumed ideal.

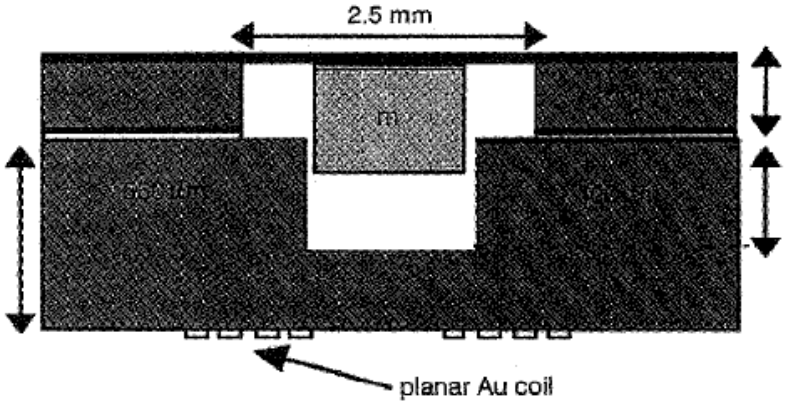

Figure 4 - Schematic diagram of the pick-up coil and flexible membrane generator [15].

Some studies around vibrating cantilevered beam generators were also explored over the years, as it is the case of [16] where a beam/magnet assembly was developed (Figure 5). The represented system consists of a mass made up of two magnets mounted on a C-shaped core in order to provide a uniform magnetic field in the air-gap, and a coil placed in the air-gap at the appropriate angles. As the housing moves, the cantilevered beam will flex and there will be a relative movement between the core and the coil, leading to energy generation.

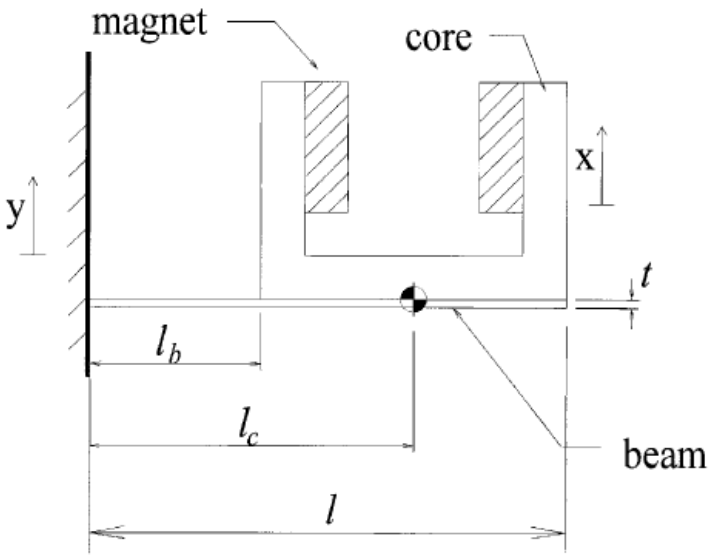

Figure 5 - Vibrating cantilevered beam generator drawing [16].

In the year of 2002 a new electric power supply system for deeply implanted medical devices was proposed (Figure 6). This system is composed of a permanent-magnet coupling and a small generator. A permanent-magnet rotor is placed on the outside (*Rotor* 1), whilst another one is implanted deeply in the inside (*Rotor* 2), having a generator attached. The rotation of *Rotor* 1 is powered by external means, inducing the rotation of *Rotor* 2 which moves the generator [17].

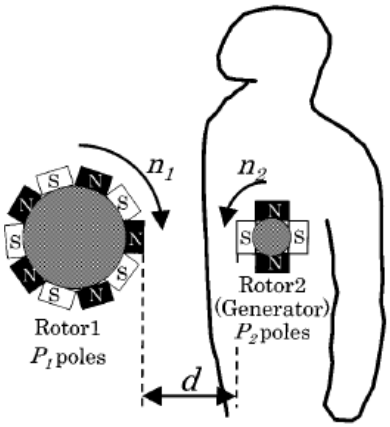

Figure 6 - Principle of the generating system for deeply implanted devices [17].

Rotary motion designs were also used in [18], with some advantages over the above described generators because it has two degrees of freedom for energy generation. Depending on the geometry and initial conditions, the mechanical excitation of the generator housing leads to rotation of the pendulum (Figure 7).

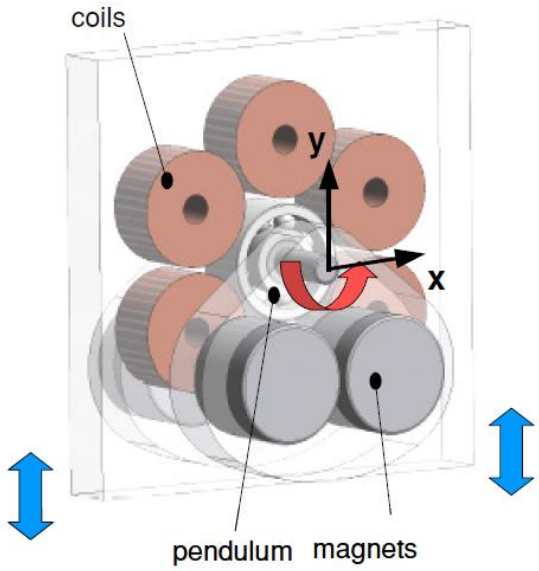

Figure 7 - Representation of the pendulum and its movement degrees of freedom [18].

These are the main concepts of micro electromagnetic systems studied by science, explored and combined with each other by numerous investigators, differently approached either in dimensioning, configuration of the electrical loads, mathematical models adopted, optimization processes, test conditions, power obtained, among other parameters in order to advance the technology.

Being so, an analysis of the parameters of best concern for this dissertation is presented in Table 1.

Table 1 – Historical review of main developed electromagnetic generators.

Generator Configuration	Dimensions	Load Configuration	Theoretical Model	Optimization methods	Test Conditions	Average power output
Williams and Yates 1996 [11]						
Mass-spring generator, the mass being a magnet which movement induces voltage in a coil.	- Mass section: 16 cm^2 - Mass: 15 mg	Resistive	Linear	Control of the damping factor.	1 μW at 70Hz and 0.1 mW at 330Hz.	
Shearwood and Yates 1997 [15]						
Magnet on a polyimide spring, moving relatively to a planar coil attached to the housing.	- Polyimide thickness: 7 μm - Magnet mass: 2.4 mg **Coil properties:** - Thickness: 2.5 μm - Number of turns: 13 - DC resistance: 35 Ω	LR System DC resistance: 39 Ω	Linear	N/A	- Frequency of vibration: 4.4 Hz - Amplitude of vibration: 500 μm	0.3 μW
Williams, Pavic et al. 1998 [12]						
Mass-spring generator, damped by the interaction coil-magnet.	- Generator volume: 1000 cm^3 - Magnet mass: 1 kg - Displacement range of the mass of up to 1 or 2 cm	N/A	Linear	N/A	- Resonant frequency of the generator: 4.5 Hz	570 μW

Generator Configuration	Dimensions	Load Configuration	Theoretical Model	Optimization methods	Test Conditions	Amount of power generated
Amirtharajah and Chandrakasan 1998 [19]						
Mass-spring generator	- Mass: 0.5 g - Spring constant: 174 N/m	First order LR system in series. Coil load resistance: 10 Ω	Linear	Manipulating the mechanical resonance of the spring-mass system to the 2Hz vibration frequency.	- Input frequency: 2 Hz - Amplitude of vibration: 2 cm (corresponding roughly to something carried in one's pocket)	400 μW
El-Hami, Glynne-Jones et al. 2001 [16]						
Point mass made up of two magnets mounted on a c-shaped core supported by a cantilever beam. Coil made up of single solid core enameled copper wires and placed between the magnets at right angles.	Generator volume: 0.24 cm^3 Coil properties: - Number of layers: 3 - Number of turns per layer: 9 - Wire diameter: 0.2 mm Mass of the magnetic core assembly: 500 mg	LR system. Load resistance matching coil resistance of 0.28 Ω.	Linear	Suggested: -Increasing the number of turns; -Arranging the coil carefully, making it shorter in length to reduce losses; -Reducing the air gap; -Increasing the magnet thickness for greater magnetic field.	Vibration frequency: 322 Hz Vibration amplitude: 25μm	0.53 mW

Generator Configuration	Dimensions	Load Configuration	Theoretical Model	Optimization methods	Test Conditions	Amount of power generated
Suzuki, Katane et al. 2002 [17]						
Consists of two rotors, one of which external to the body and the other internal. The internal rotor has associated a generator. Both have their movement coordinated by the magnetic attraction. The outer rotor has an external nature torque applied. The generator feeds AC voltage into a rechargeable battery via a rectifier and charger.	Distance between rotors: 1.5 cm Generator size: $5 \times 5 \times 1$ mm Generator diameter: 30 mm. Generator volume: 10 cm^3.	Resistive (13Ω).	N/A	Experimental examination of the relation among the distance between rotors, the output power, and the attractive force between rotors.	$Rotor$ 1 properties: Number of poles: 10 Flux density: 0.25 T Frequency: 1 Hz $Rotor$ 2 properties: Number of poles: 4 Flux density: 0.25 T Frequency: 2.5 Hz Generator properties: Number of poles: 12 Flux density: 0.15 T Frequency: 15 Hz	3.1 W
Turri, Miller et al. 2003 [20]						
Belt fastened around a waist, inside of which a flyweight suspended between two springs is in motion, allowing the device to enter into resonance with the hip movement.	Flyweight mass: 50g Flyweight displacement: 8 cm	Resistive.	Linear.	Identification of the generator optimal winding characteristic magnitudes (number of turns and layers, and diameter of the wire) in order to maximize the output for a given mechanical configuration.	Working frequency: 2 Hz	0.15 W

Generator Configuration	Dimensions	Load Configuration	Theoretical Model	Optimization methods	Test Conditions	Amount of power generated
Lee, Yuen et al. 2003 [21]						
Spring-mass system. Consists of five main components: - Inner and outer housing used to carry the resonating structure and the power resonating system, respectively; - a resonating spring; - a permanent magnet; - a copper coil; - a power-management circuit for output voltage step up and energy storing purpose.	Copper spiral spring: Spring diameter: 8mm Spring thickness: 0.1 mm	Load resistance: 1500 Ω	Linear	N/A	Input frequencies: $Below$ 100 Hz Input amplitudes: 250μm	830 μW
Kulah and Najafi 2004 [22]						
Consists of two resonating structures. One is a diaphragm suspended with a soft spring and has a low resonance frequency that is adjusted for the target application. It carries a permanent magnet composed of two pieces for both mechanical frequency up-conversion and electromagnetic power generation. The lower resonator is a cantilever beam with higher resonant frequency, and supports a coil for electromagnetic power generation.	**Micro-scale design:** - Cantilever size: $400x300x10\mu m^3$ - Coil turns: 37 - Magnet size: $2x2x1mm^3$ **Milli-scale setup:** - Cantilever size: $50x15x0.4\ \mu m^3$ - Coil turns: 3 - Magnet size: $20x20x5\ mm^3$	N/A	Linear	N/A	**Micro-scale design:** - Catch distance: 30 μm - Release distance: 100 μm - Cantilever resonating frequency: 11.4 kHz - Diaphragm resonating frequency: 10 Hz **Milli-scale setup:** - Catch distance: 11 μm - Release distance: 25 μm - Cantilever resonating frequency: $25-50\ kHz$ - Diaphragm resonating frequency: 1 Hz - Magnet movement frequency: 1Hz	**Micro-scale design:** 2.5 μW (one cantilever) **Milli-scale setup:** 4 nW

Generator Configuration	Dimensions	Load Configuration	Theoretical Model	Optimization methods	Test Conditions	Amount of power generated
Glynne-Jones, Tudor et al. 2004 [23]						
Two different cantilevered prototypes analyzed, A and B.	**Prototype A:** - Cantilever length: 1.1 cm - Cantilever width: 0.9 cm - Cantilever height: 0.85 cm - Overall volume: 0.84 cm^3 **Prototype B:** - Cantilever length: 2.1 cm - Cantilever width: 1.5 cm - Cantilever height: 1 cm - Overall volume: 3.15cm^3	**Prototype A:** Optimum load resistance: 0.6 Ω **Prototype B:** Not specified	N/A	N/A	**Prototype A:** - Beam amplitude: 0.36 mm - Device resonance frequency: 322 Hz **Prototype B:** Engine speed with a resonance peak at 3000 rev/s	**Prototype A:** 37 μW **Prototype B:** Average power: 157 μW Peak value: 3.9 mW
Ruellan, Turri et al. 2005 [13]						
Axially magnetized permanent magnet configuration, with a single phase moving coil composed of three alternate windings in series.	**Coil:** - Wire diameter: 0.2 mm - Mass: 50 g - Winding height: 31 mm - Winding interior diameter: 7 mm - Winding exterior diameter: 18 mm **Spring stiffness:** 106 N/m. **Magnet:** - Tightness: 8 mm - Interior diameter: 18 mm - Exterior diameter: 36 mm	Resistive (45Ω)	Linear	Application of an algorithm for optimization of the system parameters such as coil height, magnet and coil weights, the pole pitch, the ratio of a magnet to the pole pitch and the total height of the generator.	Frequency of vibration: 2 Hz	10 mW

Generator Configuration	Dimensions	Load Configuration	Theoretical Model	Optimization methods	Test Conditions	Amount of power generated
Arnold, Joung et al. 2005 [24]						
Consists of a rotor with an annular soft magnetic back iron and a stator with micromachined surface windings on a soft magnetic substrate. A high-speed spindle driven by compressed nitrogen is used to control the rotors.	Magnet properties: Thickness: 0.5 mm Outer diameter: 9.5 mm Inner diameter: 3.2 mm (large magnet) 5.5 mm (small magnet) Rotor-stator air gap: 100 μm	N/A	N/A	Investigation of the mechanical limitations of the rotor assembly.	Rotational speed: 225000 rpm	3.3 W
Raisigel, Cugat et al. 2005 [25]						
Consists of a permanent magnet disc rotor and a stator with an electroplated three-phase planar coil. The motion happens due to compressed air.	Planar generator properties: Diameter: 8mm Thickness: 0.5mm Number of pairs of poles: 15	Three Y-connected 50Ω resistors	N/A	N/A	Speed on magneto-pneumatic bearings: 58 000 rpm	14.6 mW
Das, Arnold et al. 2005 [26]						
Generators which are three-phase, axial flux, synchronous machines, each consisting of a multi-pole surface windings stator on a soft magnetic substrate (back iron) and a rotor with an annular permanent-magnet and soft magnetic back iron.	Back iron: Thickness: 500 μm Outer diameter: 9.525 mm Inner diameter: 3.175 mm	Resistive	N/A	N/A	Rotational speed: 120 000 rpm	1.1W

Generator Configuration	Dimensions	Load Configuration	Theoretical Model	Optimization methods	Test Conditions	Amount of power generated
Cao and Lee 2006 [27]						
Consists of a permanent magnet attached to a coil through a spring.	N/A	AC-DC rectifier Boost controller to boost the output voltage of the rectifier Feedforward control to improve the DC-DC conversion; Feedback control introduced in the feedforward control to enable the output voltage to vary with the voltage of the energy storage elements.	Linear	N/A	Frequency of vibration: $42Hz$	35 mW
Niu and Chapman 2006 [28]						
Three linear generators with different dimensions.	Number of winding turns: 1500	Voltage tripler rectifier Winding DC resistance: 66Ω Capacitors: 1000 μF	N/A	N/A	Base frequency: 2.5 Hz Frequency multiplier: 10 Internal resistance: 60 Ω Battery voltage: 11.64 V Battery internal resistance: 0.7 Ω	Arm Swing Generator: $10mW$ Up-down Body Motion Generator: 50 to 80 mW Foot motion energy harvester: 70 to 90mW

Generator Configuration	Dimensions	Load Configuration	Theoretical Model	Optimization methods	Test Conditions	Amount of power generated
Koukharenko, Beeby et al. 2006 [29]						
Mechanism with static magnets positioned on either side of a moving coil, which is located on a silicon structure designed to resonate laterally in the plane of the chip. The coil is recessed in a silicon cantilevered paddle designed to vibrate laterally in the plane of the wafer.	Volume of the device: 100 mm^3 **Simmulation:** Supporting paddle beam dimensions: Length: 1mm Thickness: 500μm Width (three different simulations): $A\ -\ 500\mu m$ $B\ -\ 400\mu m$ $C\ -\ 300\mu m$ Separation between magnet and coil: 0.1 mm **Experimental:** - Magnets dimensions: $1x1x3\ mm$ Coil: - Outer diameter: 2.4 mm - Inner diameter: 0.6 mm - Number of turns: 600 - Wire thickness: 25μm Separation between magnet and coil: 0.5mm	For simmulation: $A - Rload = 20.4\ k\Omega$ $B - Rload = 14.8k\Omega$ $C - Rload = 9.8k\Omega$	N/A	N/A	Input acceleration: 3.924 m/s^2 Input frequency: 1.615 Hz Maximum displacement of the center of the coil: 240 μm Measured resistance of the coil: 112 Ω Coil inductance: 367 μH	104 nW

Generator Configuration	Dimensions	Load Configuration	Theoretical Model	Optimization methods	Test Conditions	Amount of power generated
Constantinou, Mellor et al. 2006 [30]						
Ideal mass-spring generator.	Two tested coils: Coil A: - Length: 0.03 m - Radius: 0.01538 m - Thickness: 0.00575 m - Layers: 8 - Turns: 320 - Measured impedance: 1.54 mH Coil B: - Length: 0.0299 m - Radius: 0.01274 m - Thickness: 0.00263 m - Layers: 4 - Turns: 160 - Measured impedance: 0.331 mH	LR system.	Linear	N/A	N/A	N/A
Spreemann, Manoli et al. 2006 [18]						
Consists of a generator that converts linear into rotary motion.	- Number of pole pairs: 1 - Number of turns per coil: 150 - Remnant flux density: 1.1 T - Coil area enclosed by the boundary: 11.34 mm^2 - Internal resistance for all coils: 20Ω	N/A	Linear	N/A	Vibration amplitude: 100 μm Prototype volume: 1.5 cm^3 Prototype total weight: 2.85 g Vibration frequencies: 30 to 80 Hz Pendulum length: 440 μm	0.4 to 3 mW

Generator Configuration	Dimensions	Load Configuration	Theoretical Model	Optimization methods	Test Conditions	Amount of power generated
Beeby, Torah et al. 2007 [31]						
Mass-spring generator	Generator volume: 0.15 cm^3 Number of coil turns: 2300	Resistive ($4k\Omega$)	Linear.	Study of magnet dimensions and coil properties	Resonant frequency: 52 Hz Acceleration range: 0.19 to 3.7 m/s^2 Input frequency range: 43Hz to 109Hz	Power: 46μW Voltage: 428mV
Yuen, Lee et al. 2007 [32]						
Two micro-power transducers in series with inner structure identical to [21] and a power management circuit (consisting of a voltage multiplier and a storage capacitor), altogether in an AA sized structure.	Spring constant: 40 N/m Magnet mass: 192mg Coil wire length: 30m	Varying resistive loads (1 to 30$k\Omega$)	Linear.	N/A	First-mode resonant frequency: 72Hz System damping ratio: 0.723 Magnetic field intensity: 0.36 T Input acceleration: 4.63 m/s^2 Amplitude of vibration: 250 μm Input frequency of vibration: 70.5 Hz	AC output voltage: 450mV (of the two outputs in series) Power: 20 to 120μW

Generator Configuration	Dimensions	Load Configuration	Theoretical Model	Optimization methods	Test Conditions	Amount of power generated
von Büren and Tröster 2007 [1]						
Linear electromagnetic generator which comprises a moving part, the translator, and a stationary part, the stator. The translator consists of axially magnetized disk shaped magnets separated by soft-magnetic spacers, which act as flux concentrators and form the magnetic poles. The stator contains several armature coils. Adjacent coils are wound in different directions and connected in series.	Stator and translator volume: $0.25 cm^3$ Active volume of the generator: 0.5 cm^3 Volume of the entire housing: 30.4 cm^3	LR system	N/A	Optimization of the volume, the air-gap length, and the amplitude limit.	Frequency range: $0.1\ to\ 120 Hz$	$2\ to\ 25 \mu W$ when worn on the body during walking, depending on the position in the human body.
Saha, O'donnell et al. 2008 [14]						
Three different configurations, with axially magnetized permanent magnets placed vertically inside a tube so that facing surfaces have the same polarization. Thus the fixed magnets repel the moving one.	Magnetic pole piece thickness: $3\ mm$ Tube: $17 \times 55\ mm$ Middle magnets: $15 \times 8\ mm$ End magnets: 10×1 Coil properties: - Wire thickness: $40\ \mu m$ - Number of turns: 1000 - Moving mass: $0.027\ kg$ - Outer diameter: $18\ mm$ - Inner diameter: $17\ mm$ - Length - Wire resistance: 800 Ω	Resistive ($7.3\ k\Omega$)	Linear	N/A	Frequency range: $2\ to\ 2.75\ Hz$	$300\ \mu W\ to\ 2.5\ mW$

Generator Configuration	Dimensions	Load Configuration	Theoretical Model	Optimization methods	Test Conditions	Amount of power generated
Bowers and Arnold 2008 [33]						
Employs a spherical, unidirectionally-magnetized permanent magnet ball that is allowed to move arbitrarily in a spherical cavity wrapped with copper coil windings.	Tested devices volume: 1.5 to 4 cm^3 Number of coil turns: 400 and 600 (for the equator-wrapped design and the offset coil design, respectively) Overall system size: 0.635 to 1.91 cm diameter cavity Ball-to-cavity diameter ratio: 70%	N/A	N/A	Analysis of the dependence of the output power when varying the number of coil turns, the overall system size, and the ball-to-cavity diameter.	Walking velocity: 4 km/h Running velocity: 14 km/h	N/A
Mack, Kratt et al. 2009 [34]						
Consists of a printed circuit board with an array of 3 × 3 coils being opposed by a magnetic polydimethylsiloxane membrane with an array of 3 × 3 magnets.	Permanent magnets properties: Diameter: 1 mm Height: 0.5 mm Membrane properties: Thickness: 250 μm Diameter: 14 mm Printed circuit board thickness: 1 mm Coil windings: 25 $each$ Coil resistance: 30 Ω	Resistive (220 $k\Omega$)	N/A	N/A	Frequency: 150 Hz	Around 4.54 nW

Generator Configuration	Dimensions	Load Configuration	Theoretical Model	Optimization methods	Test Conditions	Amount of power generated
Dallago, Marchesi et al. 2010 [35]						
Consists of four magnets, two movable and two fixed, arranged in a way such that both fixed magnets repel the moving one.	N/A	Resistive (158 Ω)	Non-linear (magnetic repulsion force)	Analysis of the dependence of the output voltage with the various resistive load values.	Frequency: 9 Hz	6 mW
Morais, Silva et al. 2011 [3]						
Consists of two equally built transducers working synchronously in series.	Generator weight: 14.5 g Generator volume: 3.76 cm^3	Resistive (100 $k\Omega$)	Linear	Analysis of power evolution varying with loads and frequencies.	Walking frequency: 1,3Hz Working cycle time: 9,2 s	108,9 μW

2.3 Critical comparison between solutions

Once presented some studied solutions which in some cases are already applied as power supply for implantable medical devices, underlies the need for comparing the different solutions of electromagnetic generators.

Starting with the first presented electromagnetic solution [11], the mass-spring generator, it is indeed a compact and promising system if further explored. This solution presents a reasonable amount of generated power, an easy manufacturing process and consequently a low cost associated to its implementation.

This method has the advantage, over some of the other solutions, of not requiring external mechanisms for its functioning. Although, focusing on the total hip prosthesis implementation, as this project aims, an external magnetic field can be taken into account for when the patient is not moving, for example when sleeping or resting from the arthroplasty.

Nearly all the solutions presented consider an input frequency higher than the average gait cycle frequency, and their natural frequency (which would correspond to most magnet vibration amplitude and consequently most harvested energy) is always higher than the typical gait cycle frequency, reinforcing the need for exploring this path.

Flexible membrane generator [15] has proven to be a better choice when the situation provides a high vibration frequency and a low amplitude, which is clearly not the case when dealing with human hip motion. The same applies to cantilevered beam solutions, which additionally require a spacious environment.

Spherical solution [33] despite its low average power output in comparison to other solutions, benefits from a high compactness, and is surely a potential target of study and optimization. This system, as well as the rotational generator proposed by [18], uses not only the vertical motion of the generator, but as well horizontal and rotational, which might lead in the future to a better use of the mechanical energy from the human body.

Among the proposed systems, mass-spring and magnetic levitation solutions are emphasised for their power density and easy manufacturing, with the goal of exploiting them until they present a natural frequency that can be excited with human gait.

Chapter 3

Methodology for comparative analysis

This chapter describes the proposed electromagnetic generators, their mechanical construction and the whole structure's. The whole experimental setup for the preparation of the trials is also explained, with the respective data adjusting considerations.

3.1 Energy harvesting systems proposed

With the goal of testing different configurations of electromagnetic generators as accurately as possible, two paths were proposed: the fixation of the micro generators to an actual person's hip, assuming that the outside of the leg behaves similarly enough as the inside of the hip, dynamically speaking; and the simulation of the hip motion through a robotic arm.

Analyzing these two options, the advantages and disadvantages of each are clear, as the first one is simpler to implement but has no repeatability and the last is more data-wise precise but will always have equipment limitations, such as its range distance available for the gait cycle reproduction, or its maximum permissible acceleration.

Being so, it was defined that the most interesting path to take was the one which granted feasible and repeatable data, being the robotic arm simulation. The other solution will only be registered for quantification complement, and comparison with [3].

Now the construction of the generators and their fixation structure to the robotic arm can be projected simultaneously.

3.2 Materials and methods

As stated, the generators will be attached to a robot, namely a FANUC Robot M-6*i* MODEL B (Figure 8).

Three generators with distinct dimensions are to be built, with the goal of parameterize non-linear mathematical models, predicted to be developed in the future for optimization of the generators.

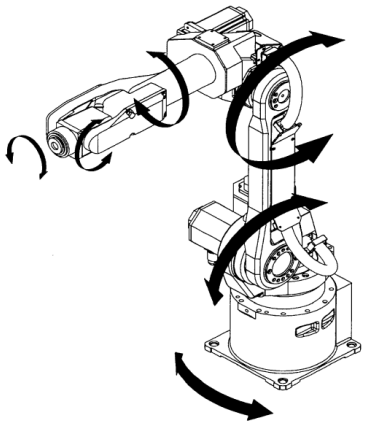

Figure 8 – FANUC Robot M-6*i* MODEL B, with operation directions of each axis represented (adapted from [36]).

3.2.1 Construction of the generators

The generator's housing has been decided to be made of Teflon (Polytetrafluoroethylene), for friction and wear reasons.

The detailed technical drawing of all three housings can be consulted in Appendix A, corresponding to the generators with 16000, 9000 and 3000 winding turns, which for the sake of an easier reading are entitled Generator 1, Generator 2 and Generator 3 respectively. For the perception of the system, a generator's housing can be observed in Figure 9.

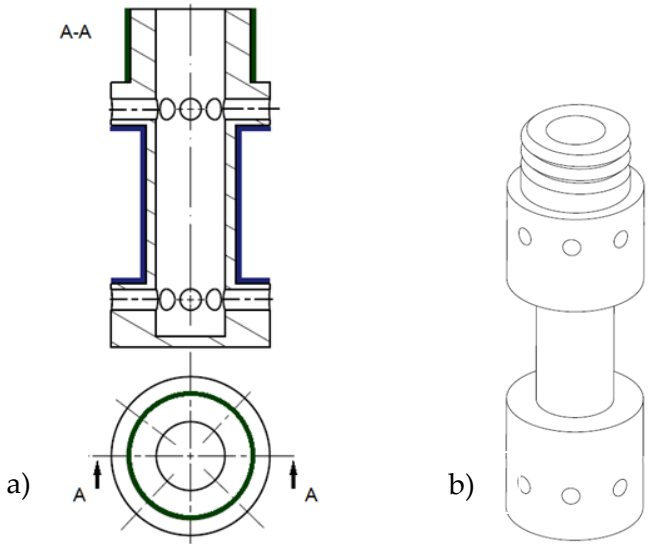

Figure 9 – a) Representative drawing of the generator's housing; b) Generator's housing 3D view.

The housing was fully manufactured on lathe, being the middle grove (Figure 9-a in blue) machined with the purpose of having an appropriate shape for the coil winding.

Small holes on the top and bottom parts of the housing, easily distinguishable on the figure, were projected in order to decrease as much as possible the air compression component, for a better motion of the magnets.

These prototypes were not designed for an actual hip prosthesis, but specifically for implementation in the robotic arm, so the upper part of the generator was screwed and linked to an extra component, composed of Nylon, represented in Figure 10.

It should be noticed from Figure 9 and 11 that matching screwed components are highlighted in green.

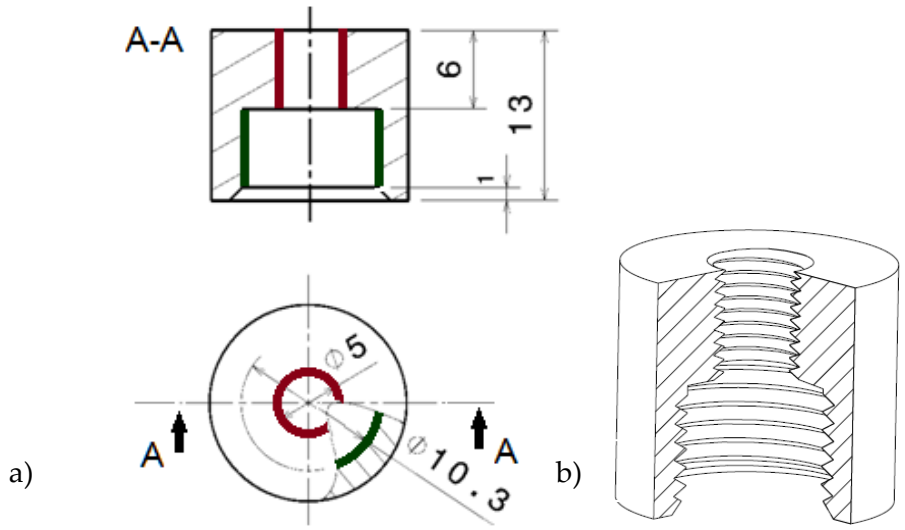

Figure 10 – Nylon cap which supports the generators (Interior screwed surfaces highlighted in green and red): a) coloured drawing and b) 3D isometric view.

The hole highlighted in red (Figure 10-a) corresponds to an interior thread, where a normalized Nylon screw (either $M6$ as shown in the figure or $M3$ for the smaller-sized generator) will assemble.

The mentioned screw has the function of fixing the whole assembly to the rest of the structure (of which construction is explained in section 3.1.2), and also has a pierce on the bottom side, where a spring will hook.

At the other end of the spring there is a small part made of Nylon (Figure 11), which will be responsible for the connection to the moving magnet. The adherence of this part to the magnet is made by a small piece of steel embedded in it, noticeable in Figure 11-a.

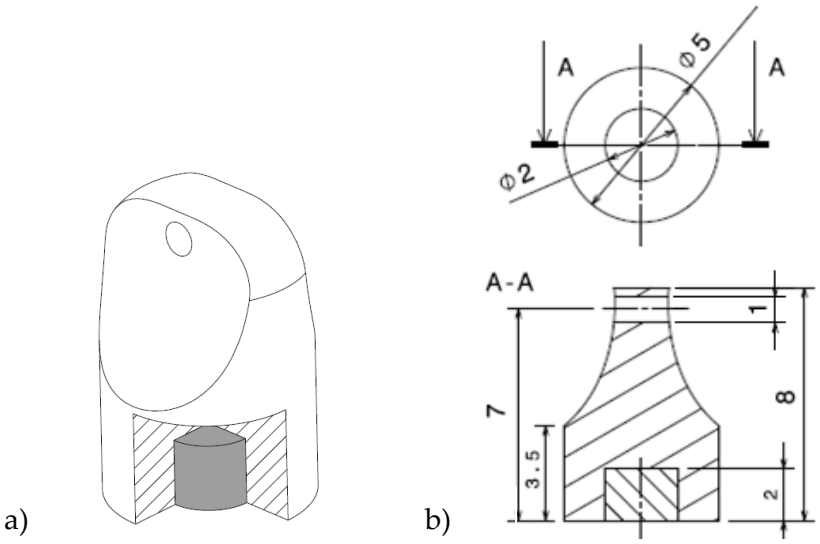

a) b)

Figure 11 – Part that connects the spring to the magnet a) 3D isometric view and b) 2D representative drawing.

The generator's design is then fully presented in Figure 12, although it will only make sense when combined with the fixation structure's design, explained in the next section.

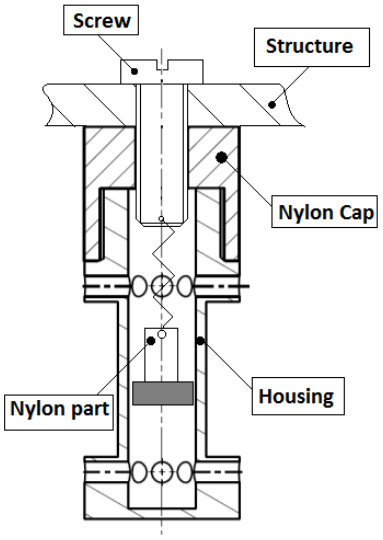

Figure 12 – Nylon cap assembled to the Teflon generator, with the normalized screw attached. The top side of the spring holds to the screw and the bottom side holds to the nylon part. The nylon part sustains the magnet.

3.2.2 Construction of the fixation structure

In order to couple the generators to the manipulator, an acrylic structure was developed. The concentricity between the devices and the robot is guaranteed by the screwed components. An assembly of all the parts of the project can be seen in Figure 13.

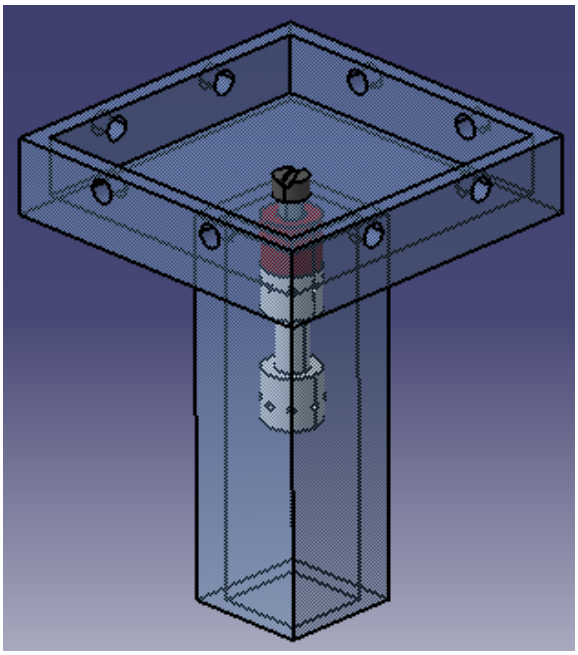

Figure 13 – Complete assembly of the fixation structure with the generator.

The acrylic construction is then connected rigidly to the robot by means of eight $M6$ screws, through the eight holes visible in Figure 13. The complete assembly can be viewed in Figure 14.

Figure 14 – Assembly of the generator fixed to the manipulator, through the acrylic fixation structure.

3.3 Experimental platform

The main objective of the experiments is the trial of the generators, namely the quantification of how much energy they can produce when travelling the distance of two human steps (one period), for posterior qualitative analysis relatively to different configurations.

In order to obtain these energy values, a DS1102 Floating-Point Controller Board from dSPACE, Inc, was used.

This apparatus outputs a signal into an industrial computer, proportional to any input voltage. This means that, if the output of the generator is connected to the input of the board, a quantification of the electric voltage can be obtained.

The connection between the generator and the board was made through coaxial cable for noise attenuation. A loading resistance of $R_l = 983\ \Omega$ is set in parallel with the generator (Figure 15) and each terminal of the generator is welded to the cable, one to the centre core and one to the metallic shield.

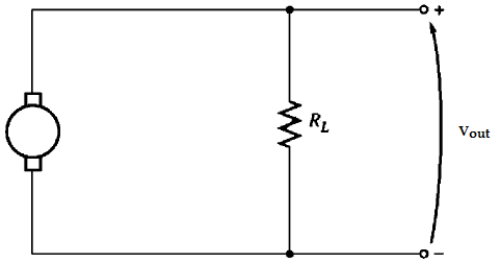

Figure 15 – Circuit of the generator with the load resistance in parallel.

A second input for the acquisition board was the voltage output of an FA201 Accelerometer (Figure 16). This sensorial device has the role of synchronizing all the data acquisition trials, implemented on the robot's tip. The beginning and end of the robot's movement is easier to identify by verifying its acceleration.

This time synchronization is explained further on, in section 3.5.

Figure 16 – FA201 accelerometer attached to the manipulator's tip.

From the reference of the accelerometer's manufacturer, it is known that the model is packaged in an anodized aluminium housing with an integral cable. The accelerometer is powered by a DC power supply.

3.4 Software

For the execution of this dissertation, three different main software platforms were used. The detailed considerations taken when using each are explained in this section.

Firstly, CATIA V5® was used for the whole mechanical projection of the platform, as well as for the technical drawings.

As for the other two programs, Matlab® from MathWorks and ControlDesk® from dSPACE are employed simultaneously.

The trajectory programming and the command of the robot (which is made through the use of Matlab®) can be observed in Appendix B and the software used for the data acquisition is executed in the real time control board, allowing the interface with the user.

A simple model in Simulink was developed for data acquisition, namely the instantaneous voltage as well as the acceleration (Figure 17), which provides read access to the two parallel A/D converters of the board into a Scope block, with a 16 bit resolution. The board data into the computer comes in tens of Volt, so in order to have a scope with a scale in Volts, a gain with a value of $k = 10$ is introduced.

A transfer function block of a first order low-pass filter, with a cut of frequency of 30 Hz is also added, in order to alternate the high frequencies in special the 50 Hz of the electrical network.

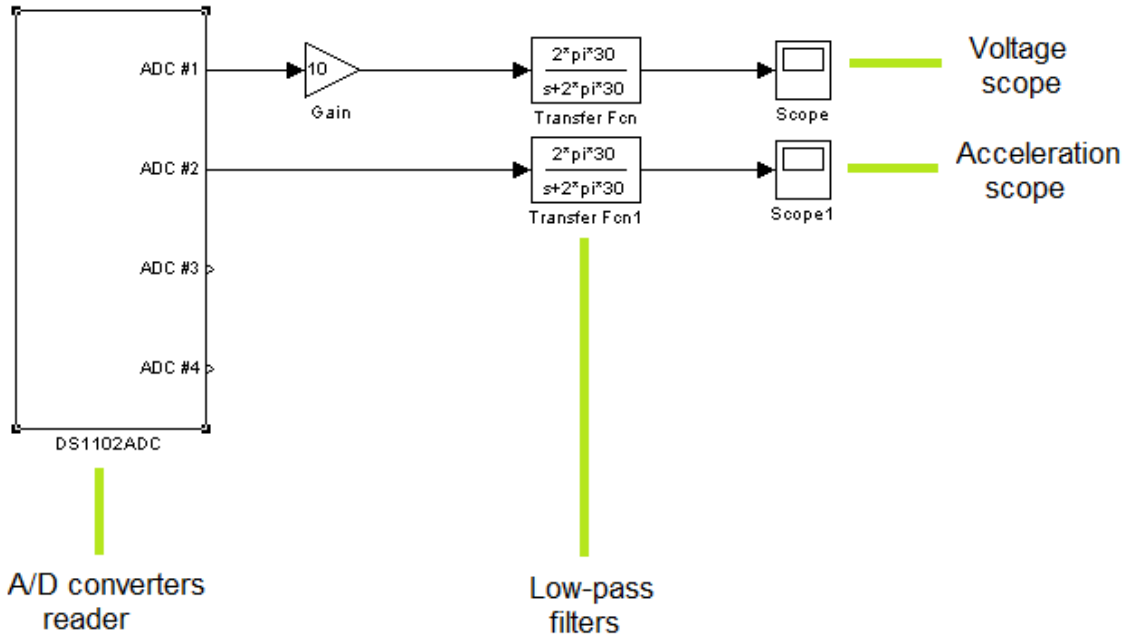

Figure 17 – Simulink model which reads the converted data coming from the control board.

In order to obtain a practical application or analysis, it is necessary to run the ControlDesk® application. This enables the development of dedicated graphic interfaces, which allows the operator to communicate with the control software that is being executed in real time. There is then the possibility, for instance, of changing the

block parameters, monitoring the behaviour of the experience or saving data for posterior processing.

For the conversion of instantaneous voltage into instantaneous power, Equation 2 is applied in Matlab® for every voltage value, and for a load resistance of 983 Ω.

$$P_{inst} = \frac{{V_{inst}}^2}{R_L} \quad (2)$$

P_{inst} – Instantaneous potency
V_{inst} – Instantaneous voltage
R_L – Load resistance

Finally, for the actual obtainment of energy for each trial, the integration of the instantaneous power of each proposed configuration was made through a Simulink model. This model can be visualized in Figure 18 and consists of a clock to output the simulation time at each step; a lookup table to map the input instantaneous power values into output values; the actual integrator; and finally a scope block.

Data acquisition was made with a step size of $1 \times 10^{-3} s$, which equals an acquisition frequency of 1 kHz.

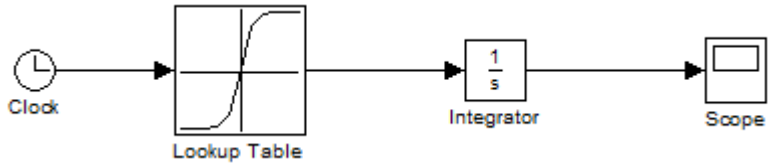

Figure 18 – Simulink model to obtain the energy through the integration of instantaneous power.

As for the ControlDesk® interface used for the simulations, a layout is created with a plotter for the voltage over time curve visualisation and a box named Capture Settings for controlling the acquisition properties. Signal 1 and signal 2 variables of the board correspond to the generator voltage and "acceleration" from the accelerometer.

a)

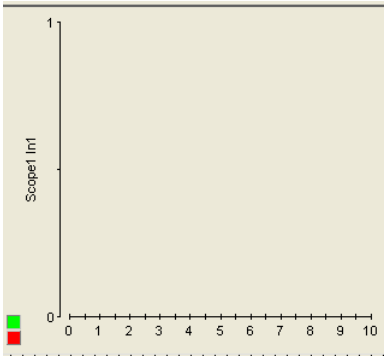

b)

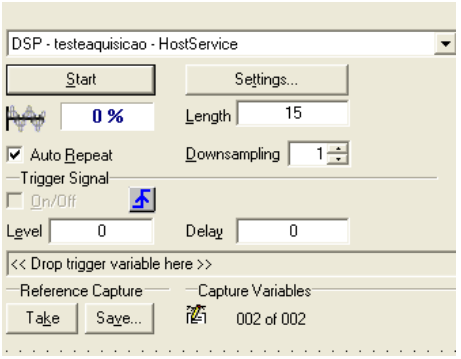

Figure 19 – ControlDesk layout: a) plotter for visualization; b) capture settings controller box for parameters manipulation.

3.5 Data adjustments

The first executed tests didn't have the low-pass filter in consideration yet, so they looked like the representation of Figure 20, which only represents instantaneous voltage's dependence over time.

Ignoring the qualitative component and merely heeding the curve behaviour, the constant noise over the whole time sample is evident, relatively to generated voltage.

From the visual perception during the real time experiment, it could be noticed that the robot motion corresponded to region *B* represented on the graph.

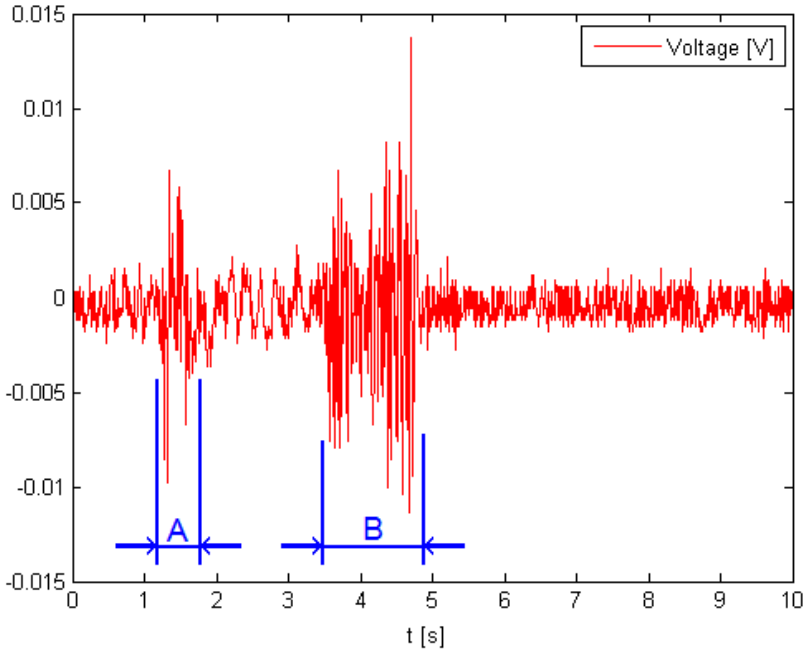

Figure 20 – Primordial plotting example of the voltage over time.

Knowing that, and with the certainty that any data outside of region B corresponds to the situation where the robot is stopped, the interrogation about the meaning of region A was inevitable. Three possibilities came to conjecture as attempt to explain this region:

- The robot's motors caused vibration on the structure when starting, making the magnet move and induce current on the generator.

- the starting of the robot motors could be pulling the energy from the electric power network, in case their feeding was too demanding, which would be felt on the control board results;

- the robot's motors, when initializing, could be producing electromagnetic noise, inducing considerable current on the generator's coil;

- all the wires and joints could not be robust or isolated enough, so they could be excessively susceptible to noise.

The simple trial of the same test, but this time without any magnets inside the generator, immediately allowed the exclusion of the first conjecture, since the same behaviour was verified, as shown in Figure 21.

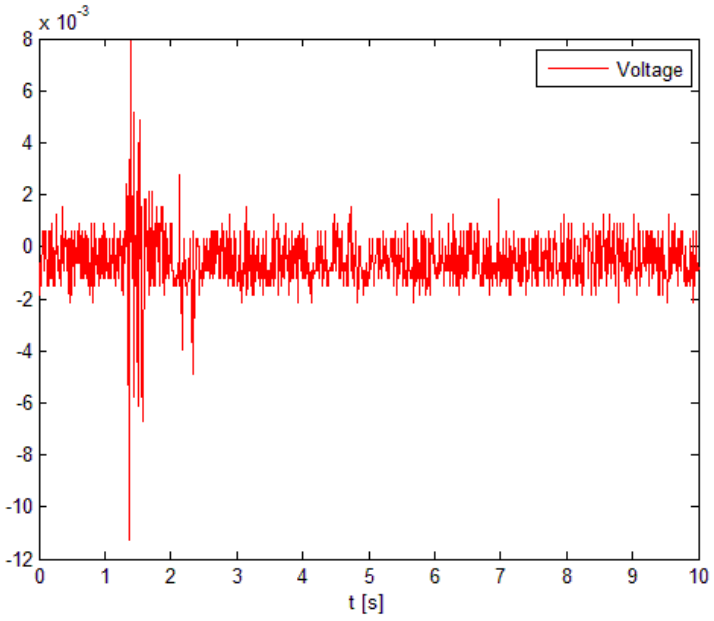

Figure 21 – Voltage plotting of the generator without any magnets inside.

The second was also proven wrong when the detachment of the generator from the manipulator made the voltage peaks disappear.

In order to refute or verify the third hypothesis, a Faraday cage was placed on the robotic arm's tip, involving the whole generator's structure, so that any electromagnetic noise coming from the exterior didn't affect the generator. Region B was also observed with this measure implemented.

Having only the last hypothesis left, all of the electric circuit connections had then to be reinforced.

The generator's terminals/load resistance/coaxial cable joints were initially screwed instead of welded for easier disassemble between tests, but, seeing the noise from Figure 21, the decision of substituting this screwed assembly by a full welded and isolated set had to be made. A new test without any magnets, this time with the reinforced and isolated circuit, was performed and is verifiable in Figure 22.

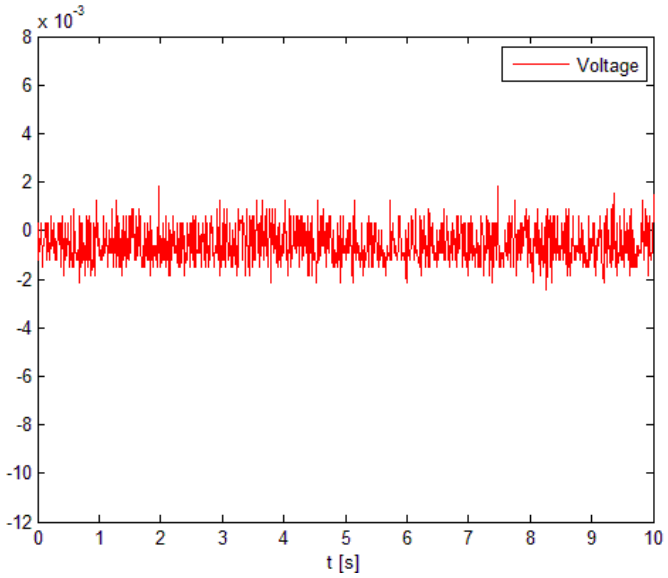

Figure 22 – Voltage plotting of the generator without any magnets inside, after the wire reinforcement and isolation.

Then the low-pass filter was decided to be implemented, and then again the test without any magnet was performed (Figure 23).

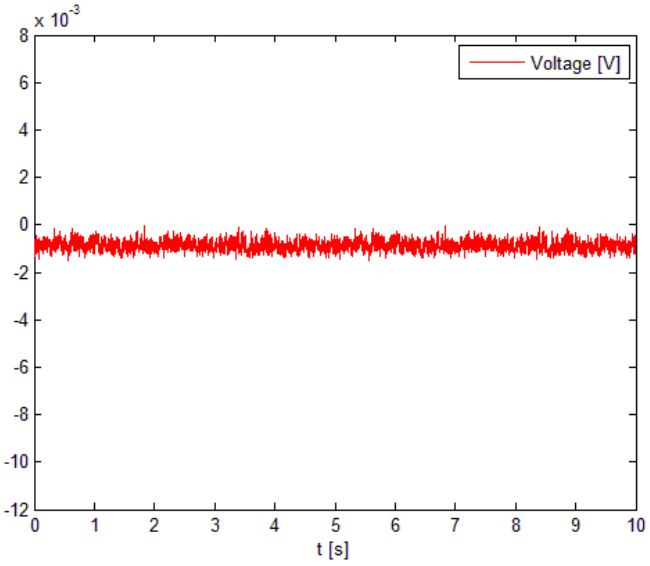

Figure 23 – Voltage plotting of the generator without any magnets inside, after the low-pass filter application.

In order to explain how the data was treated, an example of an acquired trial (Figure 24) shall be analysed. As previously stated, both generator's voltage and accelerometer's signal outputs were extracted simultaneously. The acceleration's units aren't specified because the calibration wasn't taken into account since only the curve behaviour mattered in this situation.

The starting of the acquisition was made manually through the dSPACE layout. For that reason, the accelerometer data needed to be understood at every phase (Figure 24).

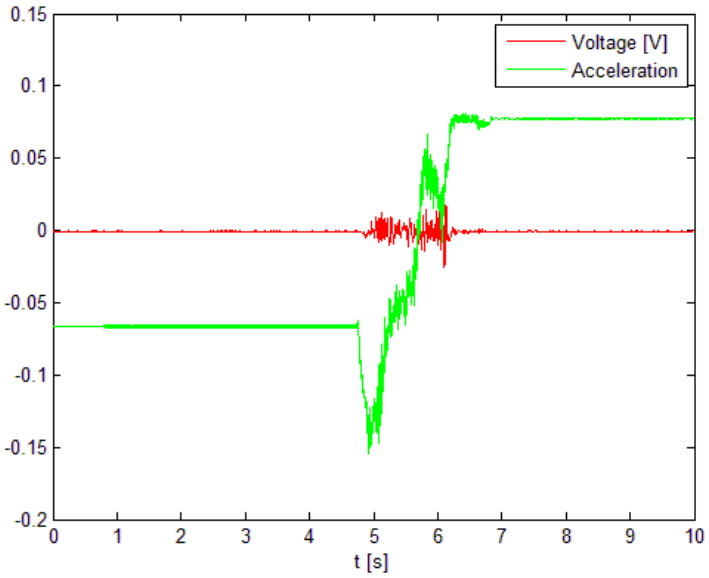

Figure 24 – Trial example, plotting both accelerometer and generator's outputs.

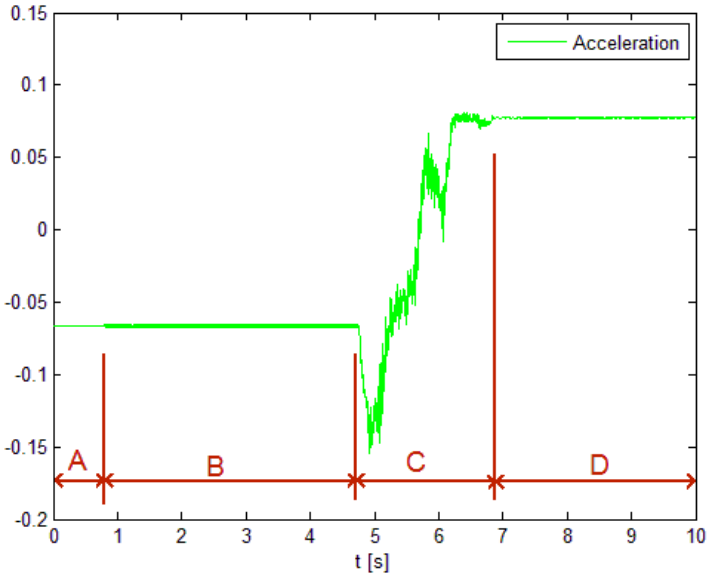

Figure 25 – Accelerometer's phases at each time interval. A – Manipulator fully stopped; B – Manipulator stopped, motors are started; C – Manipulator reproducing the hip's characteristic trajectory; D – Manipulator stops and stays still.

From the analysis of Figure 25, the restricted preference of the C region is clear, since it corresponds to the actual gait cycle period. This frontier between regions A and B was delimited by focusing on a time sample in region B (for instance between $t = 2$ and $t = 3s$ in Figure 25), and then verifying whenever the acceleration was 50% farther away from the arithmetic mean than the local minimum in that interval (Equation 3), since the first traces of acceleration show always a clear decreasing behaviour (otherwise, using only the minimum could be incorrect).

$$a_{th} = a_{min} - (a_{avg} - a_{min}) * 0{,}5 \quad (3)$$

a_{th} - Acceleration threshold between regions A and B
a_{min} – Local minimum acceleration over an interval in region B
a_{avg} – Arithmetic mean over an interval in region B

The boundary between regions C and D is then determined by adding the theoretical trajectory time duration to the time threshold between regions A and B, and also adding $0{,}24s$ in order to have enough time for the magnets to stabilize (value attributed by over-cautiousness).

The restriction of the data to region C alone is then applied for all the tests, and the values of electric voltage measured from the generator are also restricted to that interval (corresponding to the motion) (Appendix C).

Chapter 4

Experimental Trials

This chapter is intended exhibit which tests, under which conditions were performed and registered.

As previously stated, three different generators were built, classified as Generators 1, 2 and 3.

The difference between generators 1 and 2 is merely the length of the coil deposition groove, as the length in Generator 1 is 250 mm and in Generator 2 is 150 mm, which results in the discrepancy of the coil's number of turns.

The 3000 turns generator, classified as Generator 3, on the other hand, has all of its dimensions inferior to the two other prototypes, with the aim of having an additional and smaller reference for the validation of future non-linear mathematical models.

To perform a qualitative analysis, various similar tests for Generator 1 and Generator 2 were performed, and distinctly two tests for Generator 3. This choice was made because the dimensions of Generator 3, and consequently the magnets', are fully distinct from the other generators', therefore they aren't really comparable.

The tests performed are divided into two categories: mass-spring and magnetic levitation configurations. All of the configurations were also tested for two different trajectories, both correspondent to the left leg motion: walking fast and walking slowly (Appendix B.1 and B.2 respectively).

The programming of the FANUC manipulator incorporated rotations and spatial coordinates for each time increment. The trajectories used correspond to the hip motion of a single patient, who received an implant due to femoral head necrosis after a fracture [37].

Walking behaviour and mobility was good in the patient in analysis, and the implant was located in the left joint [37].

The patient is male, and had the arthroplasty at the age of 51. The measurements were made 11 months post operatively [37].

The two activities taken into account, walking fast and walking slowly, are defined by walking at a fast speed on level ground, with an average speed of 1,09 m/s, and walking at a slow average speed of 0,98 m/s, respectively [37].

Coordinates sent to the robot's tip (and coincidently spatial coordinates of the generator) are represented in Figure 26 and Figure 27 for the fast and slow trajectories, respectively.

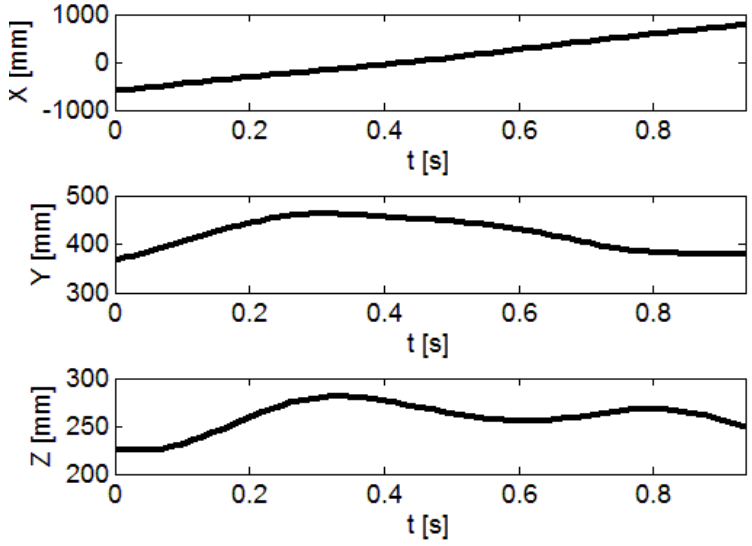

Figure 26 – Spatial coordinates sent to the manipulator. Walking fast motion.

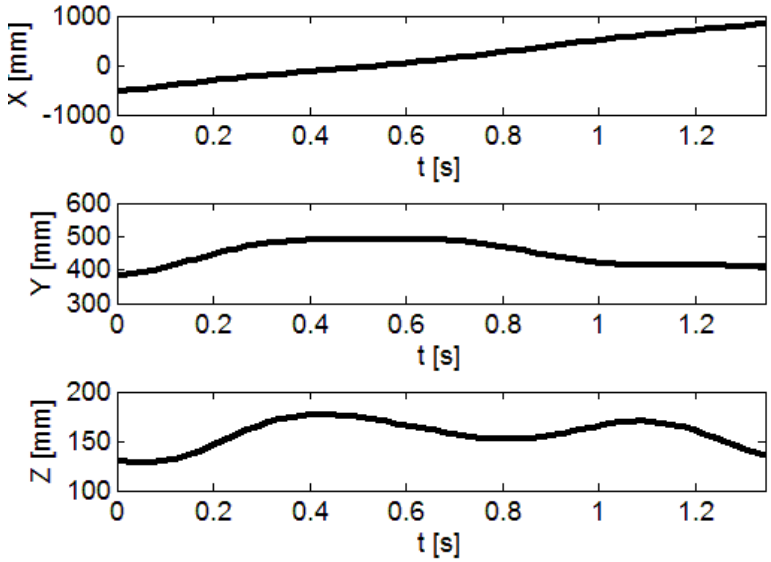

Figure 27 - Spatial coordinates sent to the manipulator. Walking slowly motion.

Also, orientations among each axis are shown in Figure 28 for fast and Figure 29 for slow trajectories.

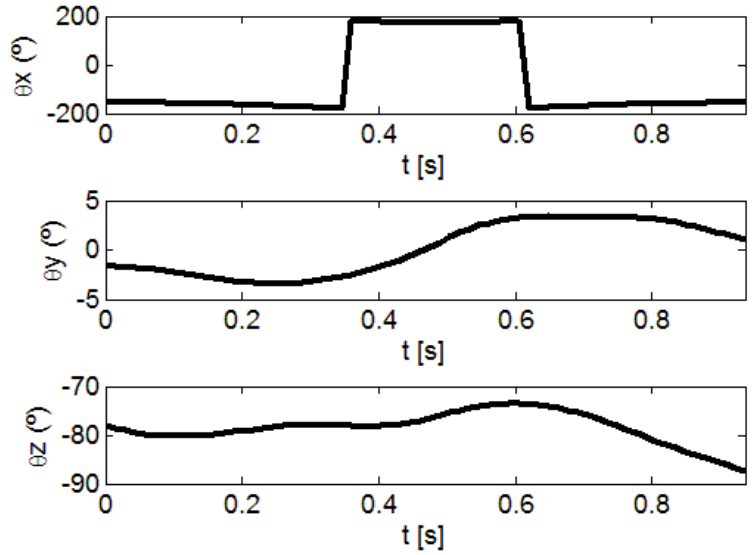

Figure 28 – Orientations around each axis, sent to the manipulator. Walking fast motion.

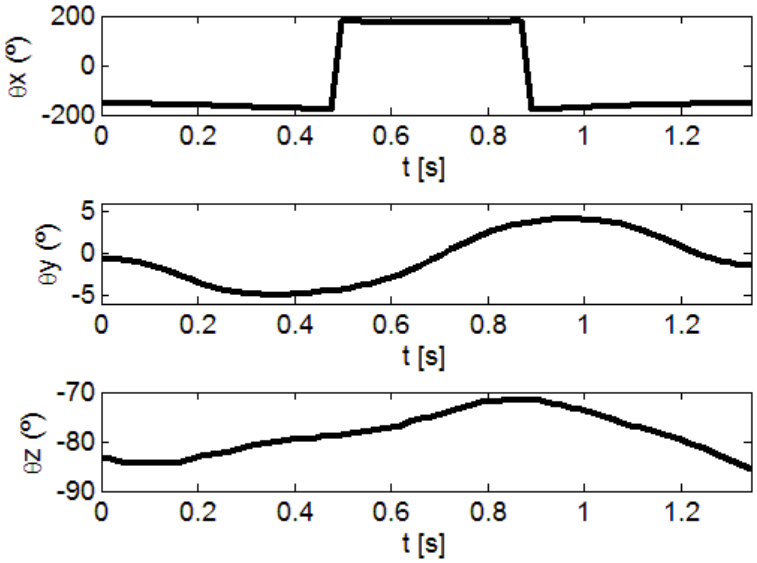

Figure 29 - Orientations around each axis, sent to the manipulator. Walking slowly motion.

The trials for the Generators 1 and 2 can now be explained, following with the trials for Generator 3.

4.1 Generators 1 and 2

Numerous tests were performed for the generators of 16000 and 9000 turns, with the focus on getting different results for different configurations, and compare the energy obtained.

There are many possible configurations but, without a system model, there is no way of knowing the ideal one, so a few were picked with the intent of helping in the validation of posterior developed models.

The magnets used for the trials were of essentially two categories, nominated Magnet A (Figure 30-a) and Magnet B (Figure 30-b).

Magnet A - Shape: $Disc$
Material: $NdFeB$
Diameter: 6 mm
Height: 6 mm
Coating: Nickel-plated $(Ni - Cu - Ni)$
Magnetisation: $N48$
Strength: 1,3 kg
Weight: 1,3 g

Magnet B : Shape: $Disc$
Material: $NdFeB$
Diameter: 6 mm
Height: 3 mm
Coating: Nickel-plated $(Ni - Cu - Ni)$
Magnetisation: $N45$
Strength: 900 g
Weight: 0,64 g

a) b)

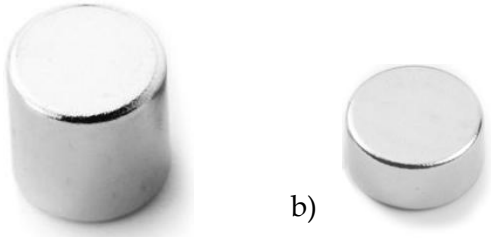

Figure 30 – Magnets used for generator's trials: a) Magnet A; b) Magnet B.

The prototypes were coiled with 0,063 mm diameter coated copper wire, with electrical resistance around $1{,}72 \times 10^{-8}\ \Omega m$ [38].

4.1.1 Mass-spring configurations

As for the spring used, it has the following properties:
Material: Copper
Length in free state: 9 mm
Number of total coils: 12
Wire diameter: 0.2 mm
Outside diameter: 4 mm
Rigidity: 2,45 N/m

Therefore, the mass-spring configurations of generators 1 and 2 tested are discriminated below in Figure 31.

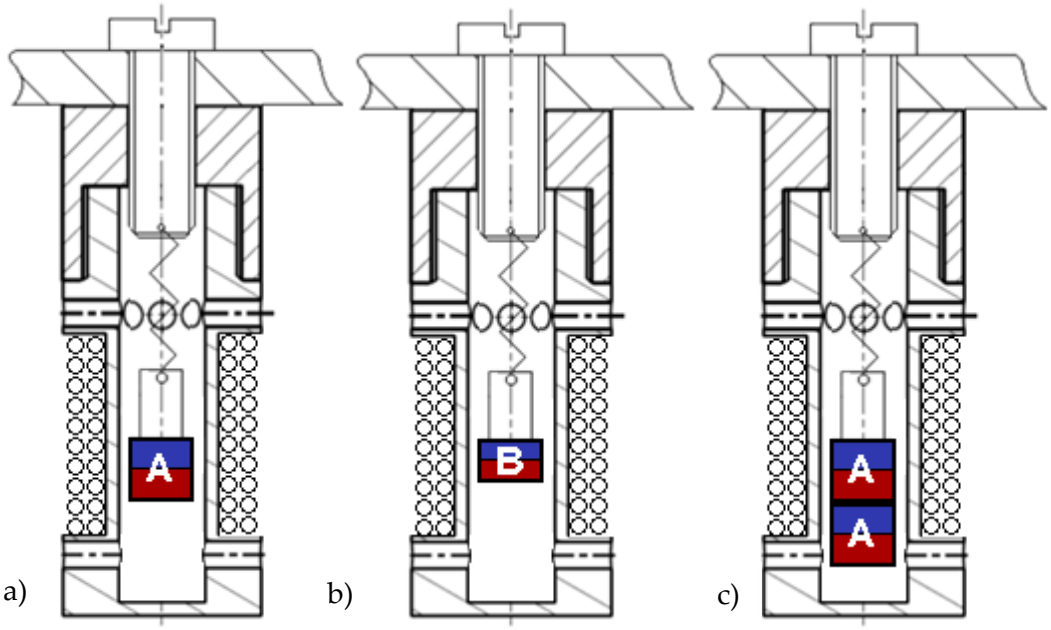

Figure 31 – Mass-spring configurations. a) One type A magnet; b) one type B magnet; c) two type A magnets.

4.1.2 Magnetic levitation configurations

In order to experiment the magnetic levitation system, the spring and the nylon part were removed. Two subcategories can be distinguished, which are the single sided magnetic levitation (Figure 32) and the double sided magnetic levitation (Figure 33).

The nylon screw which holds the generator was substituted by a metallic one for the double sided magnetic levitation configurations, in order to fix the top magnet.

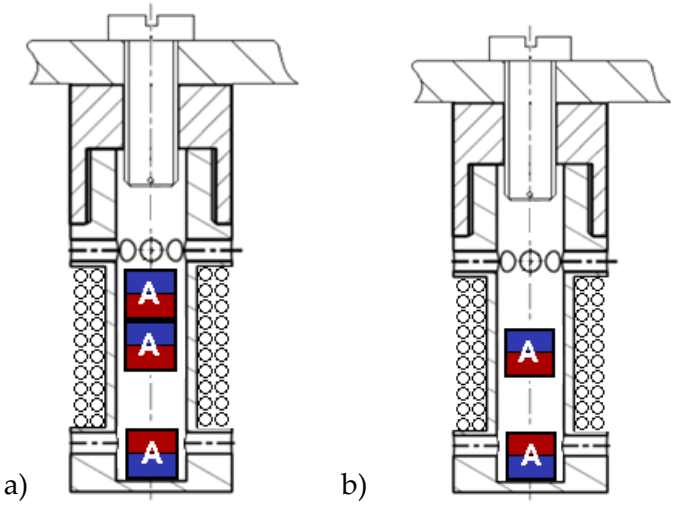

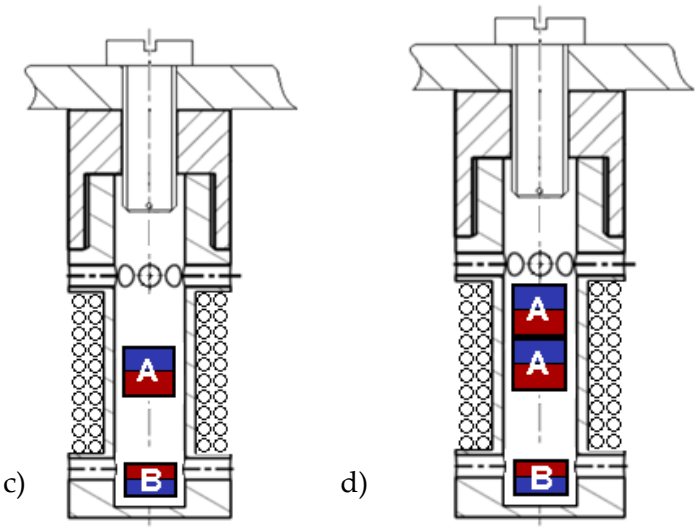

c) d)

Figure 32 – Single sided magnetic levitation configurations. a) Two type A magnets and one type A magnet; b) one type A magnet and one type A magnet; c) one type A magnet and one type B magnet; d) two type A magnets and one type B magnet.

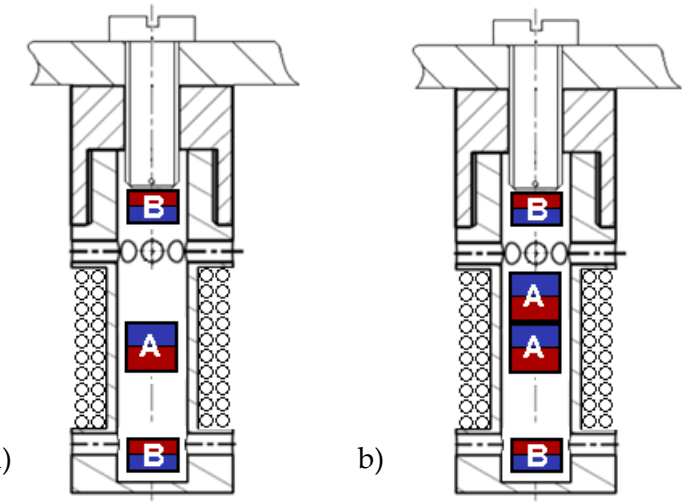

a) b)

Figure 33 – Double sided magnetic levitation configurations. a) One type B magnet, one type A magnet and one type B magnet; b) one type B magnet, two type A magnets and one type B magnet.

4.2 Generator 3

This generator was only tested for the single sided magnetic levitation configuration, for mere reference.

The present prototype was coiled with the same coated copper wire used for Generators 1 and 2, and the magnets implemented in this generator were of one type only, classified as Magnet C, with the following properties:

Magnet C - Shape: $Disc$

Material: $NdFeB$

Diameter: 3 mm

Height: 3 mm

Coating: Nickel-plated ($Ni - Cu - Ni$)

Magnetisation: $N45$

Strength: 290 g

Weight: 0,16 g

Two different configurations for this smaller generator were then experimented, visible in Figure 34-a) and Figure 34-b).

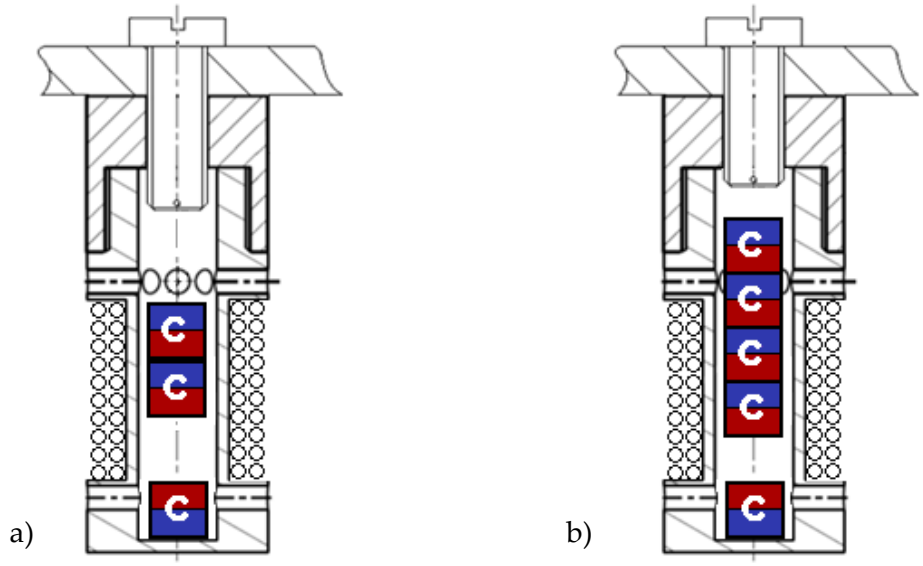

Figure 34 - Single sided magnetic levitation configurations. a) Two type C magnets and one type C magnet; b) four type C magnets and one type C magnet.

Chapter 5

Results and Comparative Analysis

This chapter exhibits the experimental results and their analysis in the context of the project objectives previously defined.

5.1 Experimental results

5.1.1 Manipulator's trials

For the most intuitive comparison, results are shown in a tabled form. The quantification of energy in nanoJoule is processed over four replications for each test, and the arithmetic average of those four tests is taken into account for comparison within each configuration, generator and trajectory.

The detailed results for the trials of each generator, configuration, and motion trajectory can be seen in Appendix D, and the simplified data, which involves the arithmetic average of each four trial repetitions, for concrete analysis, is presented in Table 2 for Generators 1 and 2, and Table 3 for Generator 3.

For presentation's sake, the configurations' terminologies are abbreviated and described in Table 4.

The plotting of the results for the configuration which got most harvested energy of all, namely $2A + 1B$ on Generator 2 with fast walking motion, is shown in Figure 35 (instant voltage quantification) and Figure 36 (instant power and energy quantification).

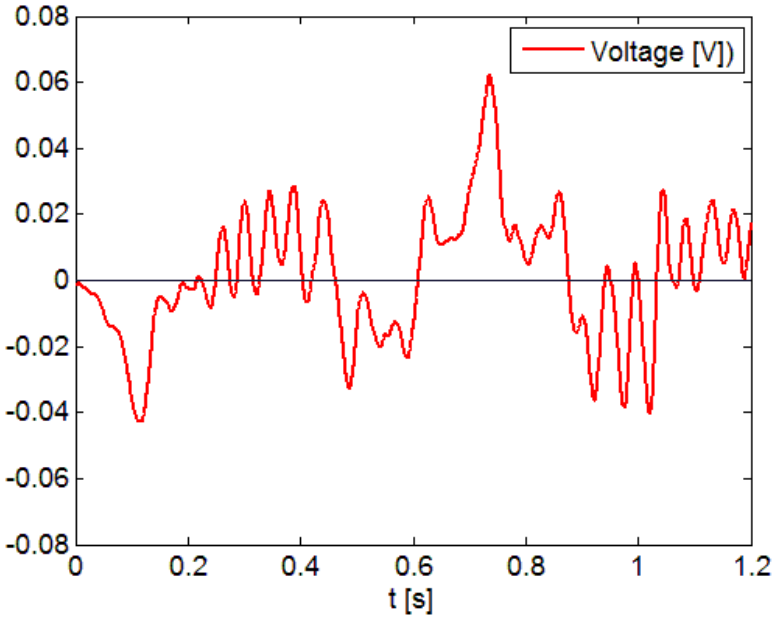

Figure 35 – Plotting of the instantaneous voltage over the time sample of the $2A + 1B$ configuration on Generator 2, fast walking.

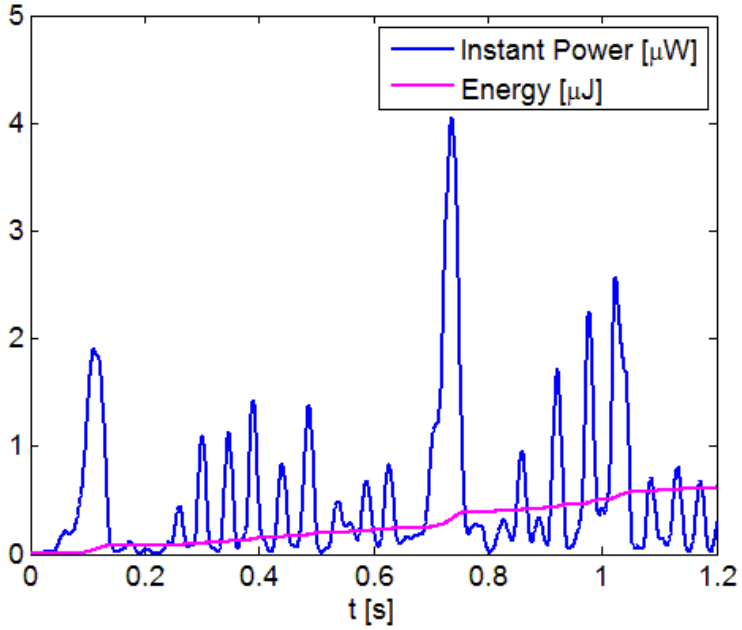

Figure 36 – Plotting of the instantaneous power over the time sample of the $2A + 1B$ configuration on Generator 2, fast walking, as well as the harvested energy.

Table 2 – Average energy harvested for Generators 1 and 2, with dependence on both trajectories and different magnet/spring configurations.

		Mass-Spring			**Single-sided magnetic levitation**				**Double-sided magnetic levitation**	
	Configuration	1A+Spring	1B+Spring	2A+Spring	1A+1A	1A+1B	2A+1A	2A+1B	1B+1A+1B	1B+2A+1B
	Average Energy $[nJ]$									
Walking Fast	Generator 1	32,6	28,4	23,8	68,9	2,83	132	8,21	1,72	2,90
	Generator 2	2,89	18,9	365	1,65	121	1,33	593	1,12	16,3
Walking Slowly	Generator 1	66,3	91,9	24,1	57,8	2,60	291	2,71	1,21	2,09
	Generator 2	4,64	65,8	568	1,65	117	12,0	471	1,29	13,2

Table 3 – Average energy harvested for Generator 3, with dependence on both trajectories and different magnet configurations.

		Single-sided magnetic levitation	
	Configuration	2C+1C	4C+1C
	Average Energy $[nJ]$		
Walking Fast	Generator 3	21,5	4,13
Walking Slowly		15,7	32,9

Table 4 – Different configurations' terminologies.

Mass-spring configurations	
1A+Spring	One type A magnet with spring.
1B+Spring	One type B magnet with spring.
2A+Spring	Two type A magnets with spring.
Single-sided magnetic levitation configurations	
1A+1A	One type A magnet levitating over one type A magnet.
1A+1B	One type A magnet levitating over one type B magnet.
2A+1A	Two type A magnets levitating over one type A magnet.
2A+1B	Two type A magnets levitating over one type B magnet.
2C+1C	Two type C magnets levitating over one type C magnet.
4C+1C	Four type C magnets levitating over one type C magnet.
Double-sided magnetic levitation configurations	
1B+1A+1B	One type A magnet levitating between two type B magnets.
1B+2A+1B	Two type A magnets levitating between two type B magnets.

5.1.2 Walking rehearse trial

An additional trial was performed, namely a walking rehearse, by attaching a generator with a certain configuration to an actual person's leg, for instance $2A + 1B$ configuration on Generator 2 (since it led to most harvested energy on the manipulator tests presented in Table 2).

This trial was performed on a male individual, 22 years old, $1{,}92\,m$ high and without implants, so the comparison with the manipulator tests is not the most righteous. Nevertheless the acquisition of this data for new reference is still constructive.

The generator was fixed to the left leg, and a linear forward trajectory was travelled for a distance of $4{,}5\,m$ over $4{,}3\,s$, which makes an average walking speed of $1{,}05\,m/s$. The trajectory was performed in five human steps, equalizing 2,5 gait cycle periods,

which over 4,3 s of motion totals a walking frequency of 0,58 Hz. The instant voltage plotting can be observed in Figure 37.

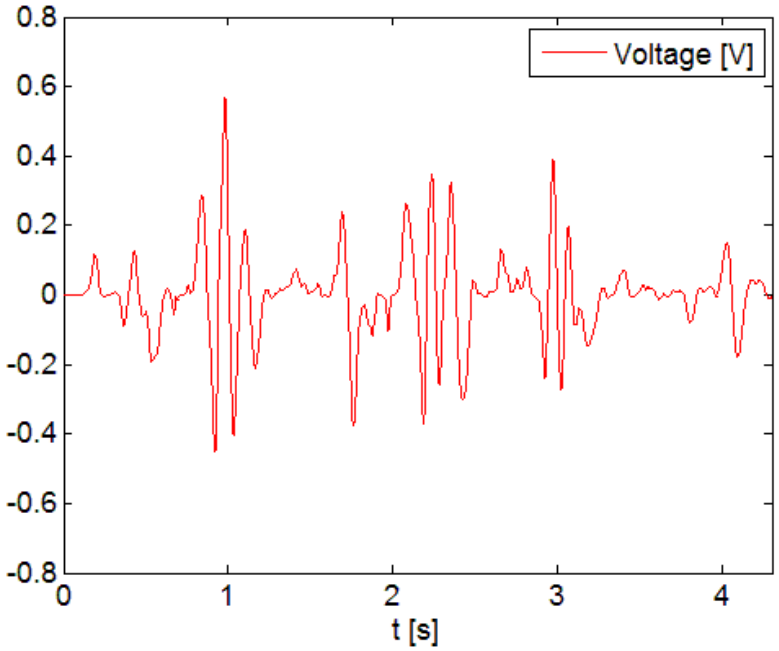

Figure 37 – Walking motion instant voltage plotting, for a walking frequency of 0,58 Hz over 4,3 s.

Resorting to the same method of power integration already described, a total harvested energy of 67,3 μJ is obtained over the whole time sample. The representation of the instant electric power as well as the energy harvested is visible in Figure 38.

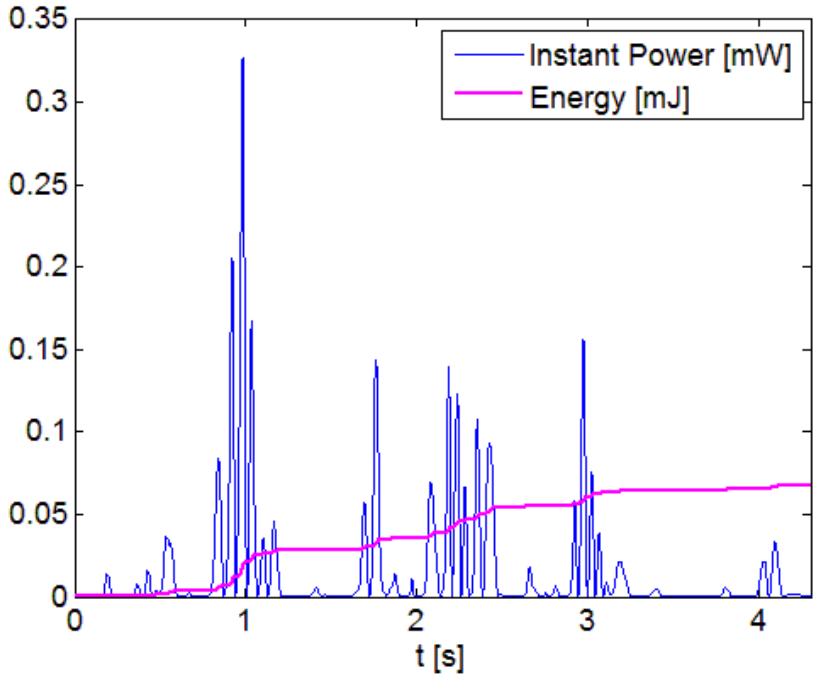

Figure 38 – Instant power (mW) and energy harvested (mJ) from the walking rehearse over the 4.3s time sample.

5.2 Comparative analysis

This section has the goal of presenting a comparative analysis between generators, their configurations and the travelled trajectories, using the information from the manipulator's trials.

At second instance, the analysis of the walking rehearse, as well as a note regarding a relation between the manipulator's trials and the actual walking test is presented.

5.2.1 Manipulator's trials analysis

The information from Table 2 is not meant to substantiate a quantification of the tests into continuous gait cycle motion, but to allow a comparative reference between different trials, configurations and trajectories, with repetitive data regarding to one gait cycle period.

The most ostentatious fact to withdraw from the data is probably that not all the generator configurations have higher energy harvesting when on fast walking motion. This can be justified by merely focusing on a person's hip motion when walking, since it is easily observable that most of the displacement occurs in directions other than the vertical, especially horizontal. Knowing this, and since the form of these generators only leverages vertical motion, it is cognizable that the faster the motion, the stronger the force of the magnets against the generator's walls, and so greater the friction.

In absolute terms, heeding only the magnetic levitation, it is verifiable that Generator 1 provided its highest energy harvest with $2A + 1A$ configuration, and Generator 2 provided its highest with $2A + 1B$ configuration. The reason for this phenomenon is obvious, as a stronger magnet on the bottom of the generator leads to a higher motion range and a weaker magnet leads to a lower motion range of the moving magnet. Since Generator 1 has a longer coil, a higher motion range will be more suitable than a lower one. On the other hand, a strong magnet on the bottom of the generator might imply too much levitation for Generator 2, and the motion of the levitating magnet might happen partially above the winding location.

Double-sided magnetic levitation has always shown to be worse than the correspondent single-sided magnetic levitation configuration (same configuration without top repelling magnets).

Generator 3 harvested more energy while on fast walking motion with configuration $2C + 1C$, but on slow walking motion harvested more energy with configuration $4C + 1C$. This might be due to the bigger contact area of the configuration $4C + 1C$, which on the fast walking motion results as a higher friction magnitude.

As a last analysis parameter, it can be noticed from the acquired data that neither the mass-spring nor the magnetic levitation configurations are notoriously better relatively to each other. It is known although that magnetic levitation is preferable in

terms of durability, since the fatigue in the spring is a critical parameter in terms of the system's lifetime.

Out of complement, in order to judge the behaviour of the different trials, some arbitrary instant voltage curves were overlapped.

The first overlap consists of a comparison between three random trials of the same configuration and same generator (Figure 39), in order to analyse the similarities and dissimilarities among theoretical replications. This configuration was randomly chosen to be $1A + 1A$, on Generator 1, with fast walking motion.

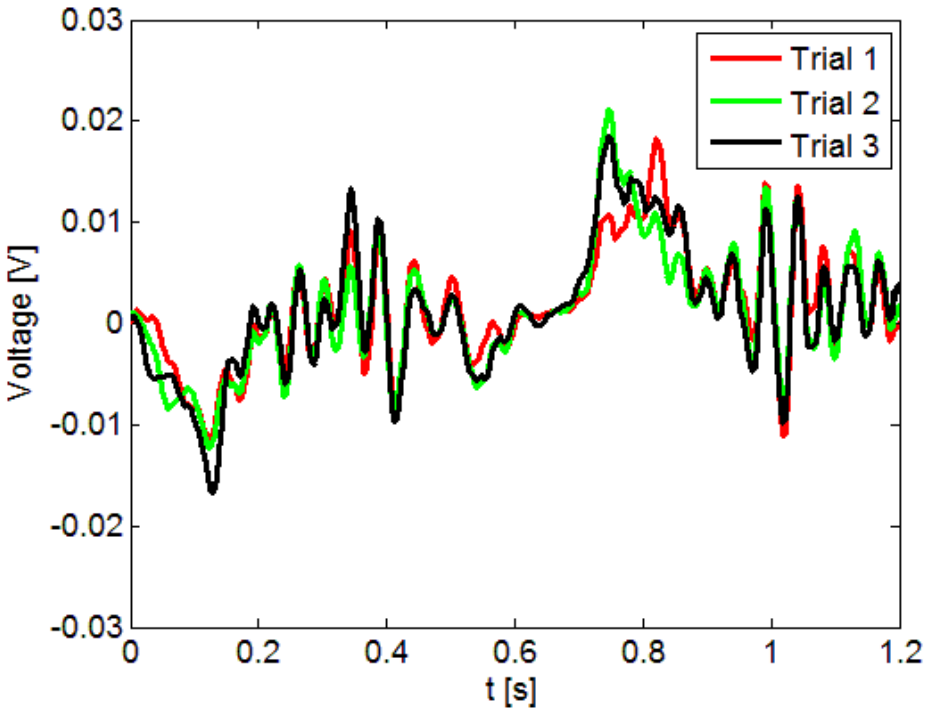

Figure 39 - Superposition of three instant voltage over time curves of three trial repetitions, for Generator 1, configuration 1A+1A.

A first instance visual analysis can be made from Figure 39, where clearly a decent degree of repeatability is present, in terms of generated voltage.

Secondly, the comparison of three random trials of different configurations, for the same generator is taken into account. These consist of three configurations for Generator 1, namely $1A + 1A$, $1B + Spring$ and $2A + 1B$, on fast walking motion (Figure 40). By abstracting from the quantification of the voltage, one can verify that the behaviour of the three curves coincides strongly in most of the time domain. One way to see it is focusing on the peaks and valleys of the plots, which are predominantly coincident.

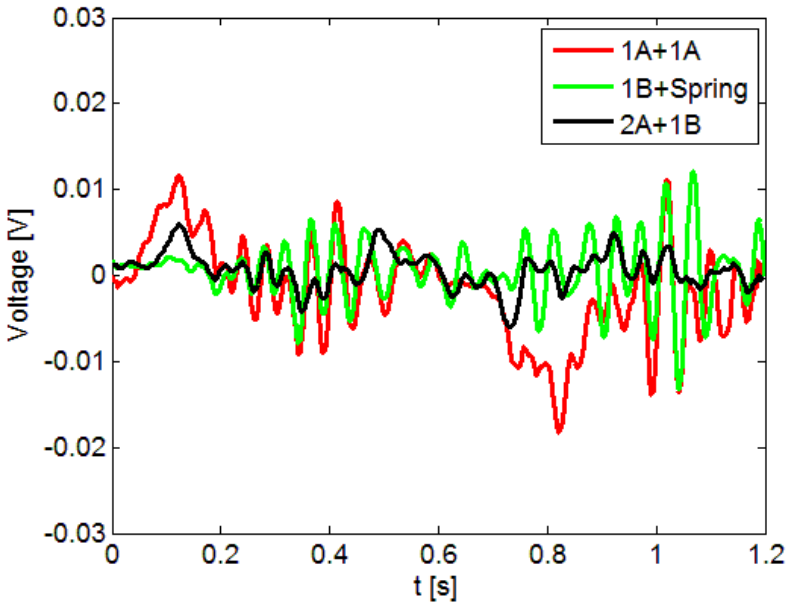

Figure 40 - Superposition of three instant voltage over time curves for Generator 1, on fast walking motion: 1A+1A, 1B+Spring and 2A+1B.

Subsequently the overlapping of two curves corresponding to the same configuration, regarding to different generators, is performed (Figure 41), and lastly the superposition between alike tests on different trajectories (Figure 42).

From the overlapping of Generators 1 and 2, it is visible that Generator 1 generally presents slightly more voltage in this trial than Generator 2. However, the superposition shows very similar behaviour among prototypes.

The lag observable between curves of Figure 42 is easily perceptible, since the movement is similar but the accelerations are distinct, which will induce altered motion of magnets.

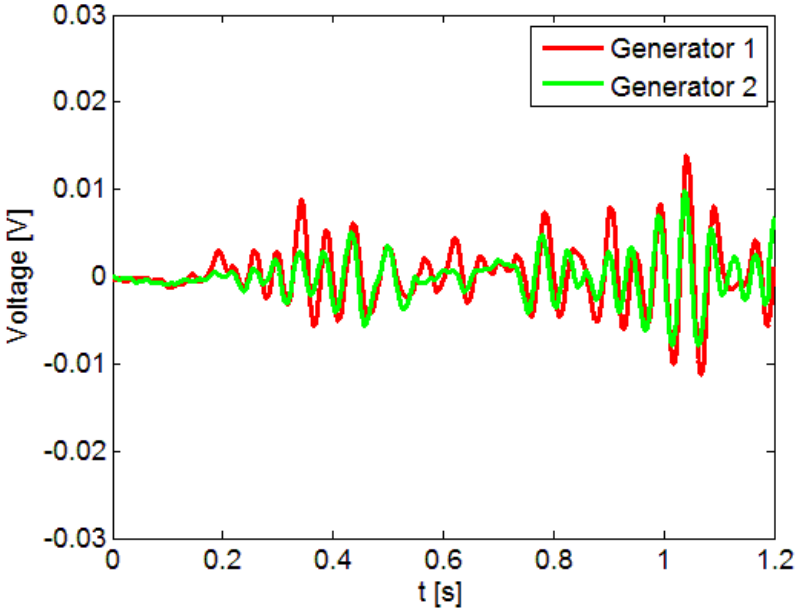

Figure 41 - Superposition of two instant voltage over time curves, of Generator 1 and Generator 2, on fast walking motion, for configuration $1P + Spring$.

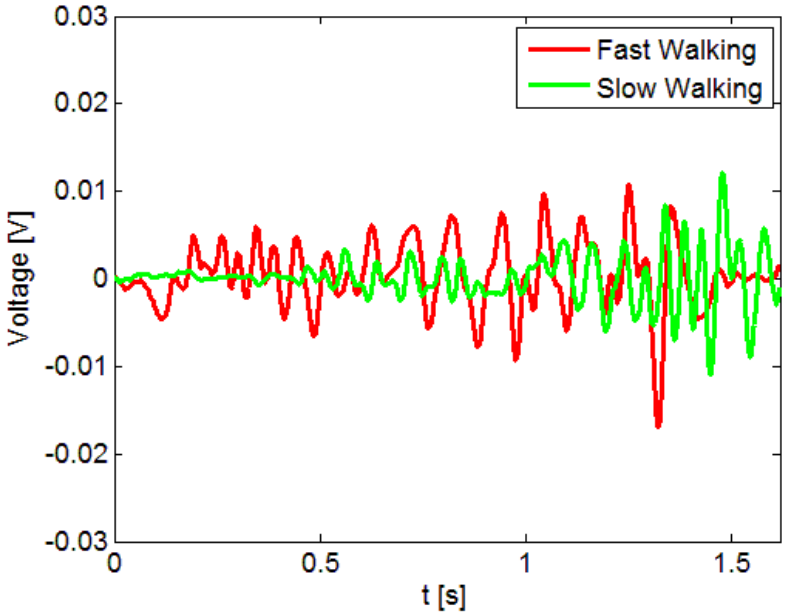

Figure 42 - Superposition of two instant voltage over time curves of Generator 1, on configuration $2A + Spring$, comparing fast and slow walking motion.

5.2.2 Walking rehearse analysis

Even after settling that the walking rehearse test performed is not analogous to the manipulator's tests due to wearer and considerations' discrepancies, the rough comparison of the best manipulator trial result ($593 \times 10^{-3}\ \mu J$ for the $2A + 1B$ configuration on Generator 2, walking fast) multiplied by 2,5 gait cycle periods relatively to the walking rehearse test can be analyzed. This multiplication results in:

$$593 \times 10^{-3} \times 2{,}5 = 1{,}48\ \mu J$$

In short, the extrapolation of the best robot trial into 2,5 gait cycle periods (similarly to the walking rehearse) offers a harvested energy value up to $\frac{67{,}3}{1{,}48} = 45{,}5$ times smaller than the obtained while attached to one's leg.

This fact might lead to some conclusions about the manipulator's tests, if assuming the differences between the two wearers studied as well as the test conditions aren't significant enough for such energy harvesting discrepancy.

The possibility implicit is that the robotic functioning attenuates the abruptions in motion that are present in human gait cycle, leading to less oscillations and posterior magnetic field variations on the generators. This fact doesn't invalidate the usage of the robotic arm, since repeatability is still only acquirable this way, and the comparative analysis between generators can still be done.

From [3], a telemetric implant is proposed, comprising three fundamental subsystems: an acquisition and data processing subsystem, an activation subsystem and an energy harvesting subsystem. Therefore, taking into account the start-up, signal conditioning, conversion, control and processing and RF transmission, and considering a working period of $300s$, there is a total energy consumption of about $360\ \mu J$ with an

average power of 1,21 μW that needs to be delivered in order to have a feasible power source.

If the multiplication of the walking rehearse energy is made, from 4,3s into a time sample of 300s, it can be assumed that this generator could harvest a total of:

$$67{,}3 \times \frac{300}{4{,}3} = 4486{,}7\mu J$$

As a preliminary analysis, this generator would then provide enough for powering these devices.

Chapter 6

Conclusions and Future Work

The work is finalized in this chapter, with comments and conclusions about the obtained results, in order to contextualize suggestions for future work and developments.

6.1 Conclusions

The developed work allowed a successful comparative analysis among different generators, their configurations and trajectories through the use of a robotic manipulator. It was possible to explain some of the results in terms of comparison, although the actual quantification can only be achieved with the parameterization of non-linear mathematical models.

The best energy harvesting result was the magnetic levitation configuration $2A + 1B$ on Generator 2 with fast walking motion which harvested $593\,nJ$ in one gait cycle period, presumably because its parameters are closer to the ideal than the other configurations'.

Although the manipulator trials provide repeatable data, a walking motion rehearse (regardless of being in slightly different conditions) shown way higher energy harvesting than these. Over 2,5 gait cycle periods an energy output of $67{,}3\,\mu J$ was obtained, while the manipulator trial energy output multiplied by 2,5 equals $1{,}48\mu J$(45,5 times smaller value). This high discrepancy leads to the conclusion that the manipulator might not be able to perform the desired accelerations correspondent to actual human gait cycle.

Regarding to the walking motion rehearse compared , the prediction of an energy harvesting of $4486{,}7\mu J$ over a time period of $300s$ is formulated, equalising an average power of $14{,}96\,\mu J$ leading to the conclusion that a telemetric implant like the one

presented in [3] could be fed with this generator. Although, it should be noted that the generator studied has a total volume of 8,83 cm^3, which is potentially more than the inside of a hip prosthesis might permit, not to mention the needed space for electronics and other elements of the smart implant.

6.2 Future Work

With this work, the construction of electromagnetic generators for smart prosthesis feeding was achieved, allowing an intensive qualitative analysis as well as a shallow quantitative analysis. It would in the future be interesting to optimize these, for a deeper analysis and consecutive structural improvement, resorting to a parameterization of the system's theoretical non-linear model.

For data reinforcement would also be necessary to study the robotic manipulator's feedback as well as the proximity between its trajectory and the theoretically equal to human hip motion, in order to explain for certainty the discrepancy between the trials and the walking rehearse performed.

While optimizing the generators, the influence of the machining parameters of the Teflon housing should be intensively studied, in order to minimize the friction with the moving magnet and potentially improving energy harvest.

Also, the structural simulation of a hip prosthesis stem could be performed, taking into account the room needed for the electronics of a smart hip implant, in order to evaluate the available volume inside of it without critically sacrificing its mechanical functions.

As it was verified, a considerable fraction of the hip movement occurs along horizontal direction, which is not leveraged with the current generator solution. Therefore an alternative system could be taken into account which takes also advantage of the horizontal motion mechanical energy, such as a pendulum or spherical solution, and further comparison with the present system could be performed.

References

1. von Büren, T. and G. Tröster, *Design and optimization of a linear vibration-driven electromagnetic micro-power generator.* Sensors and Actuators A: Physical, 2007. **135**(2): p. 765-775.
2. Pereira, L.C.M., *Geração de energia eléctrica para dispositivos médicos implantáveis*, in *Department of Mechanical Engineering*2010, Universidade de Aveiro. p. 85.
3. Morais, R., et al., *Double permanent magnet vibration power generator for smart hip prosthesis.* Sensors and Actuators A: Physical, 2011. **172**(1): p. 259-268.
4. Palacin, M.R., *Recent advances in rechargeable battery materials: a chemist's perspective.* Chemical Society Reviews, 2009. **38**(9): p. 2565-2575.
5. Yahiro, A., S. Lee, and D. Kimble, *Bioelectrochemistry: I. Enzyme utilizing bio-fuel cell studies.* Biochimica et Biophysica Acta (BBA)-Specialized Section on Biophysical Subjects, 1964. **88**(2): p. 375-383.
6. Wei, X. and J. Liu, *Power sources and electrical recharging strategies for implantable medical devices.* Frontiers of Energy and Power Engineering in China, 2008. **2**(1): p. 1-13.
7. Prutchi, D. *Nuclear Pacemakers.* [cited 2013; Available from: htttp://home,comcast.net/~dprutchi/nuclear_pacemakers.pdf.
8. Uchino, K., *Piezoelectric actuators and ultrasonic motors*. Vol. 1. 1997: Springer.
9. Platt, S.R., S. Farritor, and H. Haider, *On low-frequency electric power generation with PZT ceramics.* Mechatronics, IEEE/ASME Transactions on, 2005. **10**(2): p. 240-252.
10. Serway, R.A., J.W. Jewett, and V. Peroomian, *Physics for Scientists and Engineers, Volume 1, Chapters 1-22*2010: Brooks/Cole, Cengage Learning.
11. Williams, C. and R.B. Yates, *Analysis of a micro-electric generator for microsystems.* Sensors and Actuators A: Physical, 1996. **52**(1): p. 8-11.
12. Williams, C., et al. *Feasibility study of vibration-electric generator for bridge vibration sensors*. in *Society for Experimental Mechanics, Inc, 16 th International Modal Analysis Conference.* 1998.
13. Ruellan, M., et al. *Electromagnetic resonant generator*. in *Industry Applications Conference, 2005. Fourtieth IAS Annual Meeting. Conference Record of the 2005*. 2005. IEEE.
14. Saha, C., et al., *Electromagnetic generator for harvesting energy from human motion.* Sensors and Actuators A: Physical, 2008. **147**(1): p. 248-253.

15. Shearwood, C. and R.B. Yates, *Development of an electromagnetic microgenerator.* Electronics Letters, 1997. **33**(22): p. 1883-1884.
16. El-Hami, M., et al., *Design and fabrication of a new vibration-based electromechanical power generator.* Sensors and Actuators A: Physical, 2001. **92**(1): p. 335-342.
17. Suzuki, S.-n., et al., *Electric power-generating system using magnetic coupling for deeply implanted medical electronic devices.* Magnetics, IEEE Transactions on, 2002. **38**(5): p. 3006-3008.
18. Spreemann, D., et al., *Non-resonant vibration conversion.* Journal of Micromechanics and Microengineering, 2006. **16**(9): p. S169.
19. Amirtharajah, R. and A.P. Chandrakasan, *Self-powered signal processing using vibration-based power generation.* Solid-State Circuits, IEEE Journal of, 1998. **33**(5): p. 687-695.
20. Turri, S., et al., *Design of an electro-mechanical portable system using natural human body movements for electricity generation.* Proceeding EPE 2003, 2003.
21. Lee, J.M., et al. *Development of an AA size energy transducer with micro resonators*. in *Circuits and Systems, 2003. ISCAS'03. Proceedings of the 2003 International Symposium on*. 2003. IEEE.
22. Kulah, H. and K. Najafi. *An electromagnetic micro power generator for low-frequency environmental vibrations*. in *Micro Electro Mechanical Systems, 2004. 17th IEEE International Conference on.(MEMS)*. 2004. IEEE.
23. Glynne-Jones, P., et al., *An electromagnetic, vibration-powered generator for intelligent sensor systems.* Sensors and Actuators A: Physical, 2004. **110**(1): p. 344-349.
24. Arnold, D.P., et al. *High-speed characterization and mechanical modeling of microscale, axial-flux, permanent-magnet generators*. in *Solid-State Sensors, Actuators and Microsystems, 2005. Digest of Technical Papers. TRANSDUCERS'05. The 13th International Conference on*. 2005. IEEE.
25. Raisigel, H., et al. *Magnetic planar micro generator*. in *Solid-State Sensors, Actuators and Microsystems, 2005. Digest of Technical Papers. TRANSDUCERS'05. The 13th International Conference on*. 2005. IEEE.
26. Das, S., et al. *Multi-watt electric power from a microfabricated permanent-magnet generator*. in *Micro Electro Mechanical Systems, 2005. MEMS 2005. 18th IEEE International Conference on*. 2005. IEEE.
27. Cao, X. and Y.-K. Lee. *Design and fabrication of mini vibration power generator system for micro sensor networks*. in *Information Acquisition, 2006 IEEE International Conference on*. 2006. IEEE.
28. Niu, P. and P. Chapman. *Design and performance of linear biomechanical energy conversion devices*. in *Power Electronics Specialists Conference, 2006. PESC'06. 37th IEEE*. 2006. IEEE.
29. Koukharenko, E., et al., *Microelectromechanical systems vibration powered electromagnetic generator for wireless sensor applications.* Microsystem technologies, 2006. **12**(10-11): p. 1071-1077.
30. Constantinou, P., P. Mellor, and P. Wilcox. *Model of an electromagnetic vibration generator*. in *Universities Power Engineering Conference, 2006. UPEC'06. Proceedings of the 41st International*. 2006. IEEE.
31. Beeby, S.P., et al., *A micro electromagnetic generator for vibration energy harvesting.* Journal of Micromechanics and Microengineering, 2007. **17**(7): p. 1257.

32. Yuen, S.C., et al., *An AA-sized vibration-based microgenerator for wireless sensors.* Pervasive Computing, IEEE, 2007. **6**(1): p. 64-72.
33. Bowers, B.J. and D.P. Arnold. *Spherical magnetic generators for bio-motional energy harvesting*. in *Proceedings of the 8th International workshop on micro and nanotechnology for power generation and energy conversion applications (PowerMEMS 2008), Sendai, Japan*. 2008.
34. Mack, B., et al. *Electromagnetic micro generator array consisting of 3D micro coils opposing a magnetic PDMS membrane*. in *Solid-State Sensors, Actuators and Microsystems Conference, 2009. TRANSDUCERS 2009. International*. 2009. IEEE.
35. Dallago, E., M. Marchesi, and G. Venchi, *Analytical model of a vibrating electromagnetic harvester considering nonlinear effects.* Power Electronics, IEEE Transactions on, 2010. **25**(8): p. 1989-1997.
36. B, F.R.M.-i.M., *Maintenance Manual (B-81545EN)*, 2001.
37. Bergmann, G., et al., *Hip contact forces and gait patterns from routine activities.* Journal of Biomechanics, 2001. **34**(7): p. 859-871.
38. dos Santos, M.P.S., et al., *Multi-source Harvesting Systems for Electric Energy Generation on Smart Hip Prostheses*, in *Biomedical Engineering Systems and Technologies*2013, Springer. p. 80-96.

Appendix

Appendix A – Generators' technical drawings

Appendix B – Code of the manipulator programming on Matlab®

B.1 - Walking Fast Trajectory

```
%Variable creation
x=[];
y=[];
z=[];
t_red=[];
x_rot=[];
y_rot=[];
z_rot=[];
velocidade=[];

%Loading of the data
load('PFLWF1_hip_position.mat')

x=x_thigh_left;
y=y_thigh_left;
z=z_thigh_left;
x_rot=rotx;
y_rot=roty;
z_rot=rotz;
t_red=t;

%Repositioning of the points in space (according to the working zone
of the manipulator)
x=x*1000; %Conversion of the data into millimeters
x=x-400; %Data offset

y=y*1000; %Conversion of the data into millimeters
y=y+400; %Data offset


z=z*1000; %Conversion of the data into millimeters
z=z-600; %Data offset

% Points (X Y Z W P R)
PR=[]; % Creation of the PR vector (X Y Z W P R)

for j=1:(length(x_rot))
    PR=[PR; x(j) y(j) z(j) x_rot(j) y_rot(j) z_rot(j) 1 1 1 0 0 0];
end
```

```
% Starting of the RobCOMM server for communication with the
manipulator
robCOMM=initCOM();


% Sending of the PR vectors via TCP into the manipulator
PR_number=1;
R_number=1;

for k=1:(length(x_rot))
    string=num2str([PR_number PR(k,:)]);
    msg = sprintf('SETREG\n%s\n%s', '1', string);
    pause(0.5);
    fprintf(robCOMM.handle, msg);
    PR_number=PR_number+1;
end

for k=1:length(velocidade)
    string=num2str([R_number velocidade(k)]);
    msg = sprintf('SETREG\n%s\n%s', '3', string);
    pause(0.5);
    fprintf(robCOMM.handle, msg);
    R_number=R_number+1;
End
% Execution of the program
msg = sprintf('RUNTPP\n%s\n%s\n','DANIEL', '0');
fprintf(robCOMM.handle, msg);

% Closing of the RobCOMM  after the trial
closeCOM(robCOMM)
```

B.2 - Walking Slowly Trajectory

```
%Variable creation
x=[];
y=[];
z=[];
t_red=[];
x_rot=[];
y_rot=[];
z_rot=[];
velocidade=[];

%Loading of the data
load('PFLWS0_hip_position.mat')

x=x_thigh_left;
y=y_thigh_left;
z=z_thigh_left;
x_rot=rotx;
y_rot=roty;
z_rot=rotz;
t_red=t;

%Repositioning of the points in space (according to the working zone
of the manipulator)
x=x*1000; %Conversion of the data into millimeters
x=x-250; %Data offset
```

```
y=y*1000; %Conversion of the data into millimeters
y=y+400; %Data offset


z=z*1000; %Conversion of the data into millimeters
z=z-700; %Data offset


% Points (X Y Z W P R)
PR=[]; % Creation of the PR vector

for j=1:(length(x_rot))
    PR=[PR; x(j) y(j) z(j) x_rot(j) y_rot(j) z_rot(j) 1 1 1 0 0 0];
end


% Starting of the RobCOMM server for communication with the
manipulator
robCOMM=initCOM();


% Sending of the PR vectors via TCP into the manipulator
PR_number=1;
R_number=1;

for k=1:(length(x_rot))
    string=num2str([PR_number PR(k,:)]);
    msg = sprintf('SETREG\n%s\n%s', '1', string);
    pause(0.5);
    fprintf(robCOMM.handle, msg);
    PR_number=PR_number+1;
end

for k=1:length(velocidade)
    string=num2str([R_number velocidade(k)]);
    msg = sprintf('SETREG\n%s\n%s', '3', string);
    pause(0.5);
    fprintf(robCOMM.handle, msg);
    R_number=R_number+1;
End
% Execution of the program
msg = sprintf('RUNTPP\n%s\n%s\n','DANIEL', '0');
fprintf(robCOMM.handle, msg);

% Closing of the RobCOMM  after the trial
closeCOM(robCOMM)
```

Appendix C – Code of the data synchronization in time on Matlab®

```
% Load of the trial .mat file saved from ControlDesk
load 2A+1B_Trial1
t=A_1B_Trial1.X.Data; % time data
v=A_1B_Trial1.Y(1).Data; % voltage data
acc=A_1B_Trial1.Y(2).Data; % acceleration data

% Load resistance
Rc=983;

% Instantaneous power
P=v.*v/Rc;

pos1=find(t==2); % position where t=2s
pos2=find(t==3); % position where t=3s

A=acc(pos1:pos2);

Min=min(A);
Avg=mean(A);

% Acceleration threshold
aTh=Min-(Avg-Min)*0.5;
Th=min(find(acc<=aTh));
Th=round(Th*1000)/1000;
k=t(Th)+1.2; % 1.2= 0.96s of theoretical tima for the trajectory +
0.24s for stabilization (over-cautiousness value)

k=round(k*1000)/1000;
K=find(t==k);

% Synchronised variables
vSync=v(Th:K);
PSync=vSync.*vSync./Rc;
tSync=t(Th:K);
tSync=tSync-tSync(1); % offset of the initial time value to t=0s
```

Appendix D – Harvested energy for each trial

D.1 - Walking Fast

D.1.1 – Mass-spring configurations

Table 5 — Energy harvest for mass-spring configurations on Generator 1, walking fast trajectory.

Generator 1			
Configuration	1A+Spring	1B+Spring	2A+Spring
	Energy [nJ]		
Test 1	32,8	28,2	22,7
Test 2	35,8	28,6	21,7
Test 3	31,8	29,0	26,5
Test 4	29,8	27,9	24,2
Average	32,6	28,4	23,8

Table 6 – Energy harvest for mass-spring configurations on Generator 2, walking fast trajectory.

Generator 2			
Configuration	1A+Spring	1B+Spring	2A+Spring
	Energy [nJ]		
Test 1	2,69	19,1	362
Test 2	2,70	17,7	319
Test 3	2,99	20,1	360
Test 4	3,17	18,6	419
Average	2,89	18,9	365

D.1.2 – Single-sided magnetic levitation configurations

Table 7 – Energy harvest for single-sided magnetic levitation configurations on Generator 1, walking fast trajectory.

Generator 1				
Configuration	1A+1A	1A+1B	2A+1A	2A+1B
	Energy [nJ]			
Test 1	64,9	3,07	125	8,30
Test 2	69,3	2,68	132	8,07
Test 3	75,8	2,59	136	7,25
Test 4	65,7	2,96	134	9,22
Average	68,9	2,83	132	8,21

Table 8 - Energy harvest for single-sided magnetic levitation configurations on Generator 2, walking fast trajectory.

Generator 2				
Configuration	1A+1A	1A+1B	2A+1A	2A+1B
	Energy [nJ]			
Test 1	1,51	115	1,15	616
Test 2	1,79	116	1,29	585
Test 3	1,60	144	1,37	554
Test 4	1,70	110	1,49	617
Average	1,65	121	1,33	593

Table 9 - Energy harvest for single-sided magnetic levitation configurations on Generator 3, walking fast trajectory.

Generator 3		
Configuration	2C+1C	4C+1C
	Energy [nJ]	
Test 1	7,52	23,3
Test 2	2,10	22,2
Test 3	1,86	20,7
Test 4	5,03	19,6
Average	4,13	21,5

D.1.3 - Double-sided magnetic levitation configurations

Table 10 – Energy harvest for double-sided magnetic levitation configurations on Generator 1, walking fast trajectory.

Generator 1		
Configuration	1B+1A+1B	1B+2A+1B
	Energy $[nJ]$	
Test 1	1,78	2,95
Test 2	1,75	2,93
Test 3	1,70	2,80
Test 4	1,65	2,91
Average	1,72	2,90

Table 11 – Energy harvest for double-sided magnetic levitation configurations on Generator 2, walking fast trajectory.

Generator 2		
Configuration	1B+1A+1B	1B+2A+1B
	Energy $[nJ]$	
Test 1	1,11	22,9
Test 2	1,09	15,9
Test 3	1,17	13,8
Test 4	1,10	12,4
Average	1,12	16,3

D.2 - Walking Slowly

D.2.1 – Mass-spring configurations

Table 12 - Energy harvest for mass-spring configurations on Generator 1, walking slowly trajectory.

Generator 1			
Configuration	1A+Spring	1B+Spring	2A+Spring
	Energy $[nJ]$		
Test 1	72,5	75,5	29,5
Test 2	55,5	104	23,5
Test 3	62,4	90,6	19,7
Test 4	74,8	97,3	23,7
Average	66,3	91,9	24,1

Table 13 - Energy harvest for mass-spring configurations on Generator 2, walking slowly trajectory.

Generator 2			
Configuration	1A+Spring	1B+Spring	2A+Spring
	Energy [nJ]		
Test 1	5,52	54,5	554
Test 2	4,99	72,9	558
Test 3	4,37	67,7	613
Test 4	3,69	67,9	547
Average	4,64	65,8	568

D.2.2 – Single-sided magnetic levitation configurations

Table 14 - Energy harvest for single-sided magnetic levitation configurations on Generator 1, walking slowly trajectory.

Generator 1				
Configuration	1A+1A	1A+1B	2A+1A	2A+1B
	Energy [nJ]			
Test 1	62,3	2,20	269	6,22
Test 2	56,2	3,42	314	6,85
Test 3	58,0	2,76	299	6,48
Test 4	54,6	2,03	280	7,30
Average	57,8	2,60	291	6,71

Table 15 - Energy harvest for single-sided magnetic levitation configurations on Generator 2, walking slowly trajectory.

Generator 2				
Configuration	1A+1A	1A+1B	2A+1A	2A+1B
	Energy [nJ]			
Test 1	1,64	117	19,3	488
Test 2	1,67	127	10,3	474
Test 3	1,57	110	9,43	498
Test 4	1,72	113	8,86	423
Average	1,65	117	12,0	471

Table 16 - Energy harvest for single-sided magnetic levitation configurations on Generator 3, walking slowly trajectory.

Generator 3		
Configuration	2C+1C	4C+1C
	Energy [nJ]	
Test 1	22,3	24,4
Test 2	14,3	53,7
Test 3	13,7	27,0
Test 4	12,6	26,4
Average	15,7	32,9

D.2.3 – Double-sided magnetic levitation configurations

Table 17 - Energy harvest for double-sided magnetic levitation configurations on Generator 1, walking slowly trajectory.

Generator 1		
Configuration	1B+1A+1B	1B+2A+1B
	Energy [nJ]	
Test 1	1,27	2,07
Test 2	1,25	1,97
Test 3	1,12	2,09
Test 4	1,20	2,24
Average	1,21	2,09

Table 18 - Energy harvest for double-sided magnetic levitation configurations on Generator 2, walking slowly trajectory.

Generator 2		
Configuration	1B+1A+1B	1B+2A+1B
	Energy [nJ]	
Test 1	1,31	12,5
Test 2	1,28	11,4
Test 3	1,36	10,8
Test 4	1,21	18,1
Average	1,29	13,2